A model of the checkpoint response of the cell cycle of frog-egg extracts in the presence of unreplicated DNA.

Amit Dravid

Thesis submitted to the Faculty of the
Virginia Polytechnic Institute and State University
in partial fulfillment of the requirements for the degree of

Master of Science
in
Mathematics

John J. Tyson, Chair
Terry L. Herdman, Co-Chair
Jill C. Sible
Jeffrey Borggaard

December 9, 2004
Blacksburg, Virginia, U.S.A.

Keywords: cell cycle, frog egg extracts, unreplicated DNA, checkpoint, Chk1, wiring diagram, computational modeling, ordinary differential equations

A model of the checkpoint response of the cell cycle of frog-egg extracts in the presence of unreplicated DNA.

Amit Dravid

(ABSTRACT)

The cell cycle of eukaryotes consists of alternation between growth and DNA replication (interphase), and DNA distribution and cell-division (mitosis or M-phase). This process is regulated by a complex network of biochemical reactions. A core part of this network, called the "Cell Cycle engine" is evolutionarily conserved. The dimer of CDK1 (a protein kinase) and Cyclin proteins (the regulatory components), called M-phase Promoting Factor (MPF), and its key regulatory proteins Cdc25 and Wee1, are central parts of this cell cycle engine. Maintaining the fidelity of the DNA during the cell cycle is critical for successful propagation of the cell lineage. In the presence of unreplicated DNA, the cell cycle engine's progress into mitosis is slowed down (or halted) by regulation of MPF activity through Cdc25 and Wee1. This regulatory event, called the unreplicated DNA checkpoint, was modeled in a rudimentary fashion in the Novak and Tyson (1993) model of frog eggs. Since then, many new experiments have uncovered relevant parts of this network. Here, we include these parts into a detailed model of the unreplicated DNA checkpoint in the cell cycle of frog-egg extracts. This work and future studies of the unreplicated DNA checkpoint will lead to its better understanding and hopefully to some strategies for tackling cancer.

This work was supported by grants from NIH (Supplement to R01 59688) to Dr. Jill C. Sible and from DARPA (AFRL #F30602-01-2-0572) to Dr. John J. Tyson.

Acknowledgments

Members of both Tyson and Sible lab were extremely helpful in making of this model. With an undergraduate degree in Electrical Engineering, I was a newcomer to the field of Computational Biology when I joined the Tyson lab. Dr. John Tyson has been instrumental and extremely patient in teaching me his brand of the 'art' of computational biology, and other values of a careful scientist. Dr. Jill Sible has helped much with the understanding of experimental articles and evidence. Her enthusiasm for collaborating with computational modelers has been very supportive. Jason Zwolak helped with using his parameter optimization software. Ian Auckland was extremely helpful in the careful evaluation of experimental evidence. Emery, Mohsen, Battogtokh, and Atilla helped in various significant ways. Kathy's enthusiasm and hard work were an inspiration during difficult times. I am grateful to Dr. Terry Herdman and Dr. Jeffrey Borggaard to be on this M.S. committee and for their guidance as I pursued a M.S. in Mathematics from a background in Electrical Engineering.

Contents

List of Figures

List of Tables

Chapter 1

Introduction and background to the problem

We start with the description of the cell cycle and its checkpoint mechanisms. The experimental system, which is an *in-vitro* model of the *in-vivo* cell cycle is then described. Then, a preliminary attempt at the current problem made by Novak and Tyson (1993) is described, before giving a broad outline of how the present model was created. Subsequent chapters provide more details of the experiments and the model making (and testing) process.

1.1 The cell cycle and its checkpoints

A main characteristic of life is reproduction. We may agree that cells are the basic, self-contained units of life. The cell cycle is a cyclic process of cellular reproduction. It consists of alternation between growth and DNA replication (interphase - S phase), and DNA distribution and cell-division (mitosis - M phase). These phases may be separated by time gaps, denoted by the G1 and G2 gap phases. Interphase includes the G1, S, and G2 phases (Fig.[1.1]). During the G1 phase, the cell prepares for DNA synthesis (in S phase) by synthesizing RNA and proteins. The G2 phase appears to allow for checking the fidelity of S phase before committing to mitosis. Rapidly replicating human cells take about 24 hours to go through the cell cycle: G1 - 9 hours; S - 10 hours; G2 - 4.5 hours; M - 30 minutes. Embryonic fruit-fly cells take about 11 minutes, frog-eggs about 30 minutes, and yeast about 90 minutes per cycle. Under a microscope, M phase is the most spectacular phase of the cell cycle where one can see the condensed chromatids aligned in the middle before separation (Fig.[1.2]). Figure [1.3] shows a schematic of main events. (See Lodish et al. (2003, Ch. 21) for a both broader, and detailed exposition of the cell cycle.)

The study of various eukaryotes – especially yeast, frogs, and mammals – has led to the discovery of a central, evolutionarily conserved mechanism underlying the cell cycle. This similarity extends down to many details, like the similarity of the amino-acid sequence of the molecules attributed with similar functions (for instance, the MPF molecule).

Heterodimers of cyclin and cyclin dependent kinase (CDK) proteins are believed to be the core

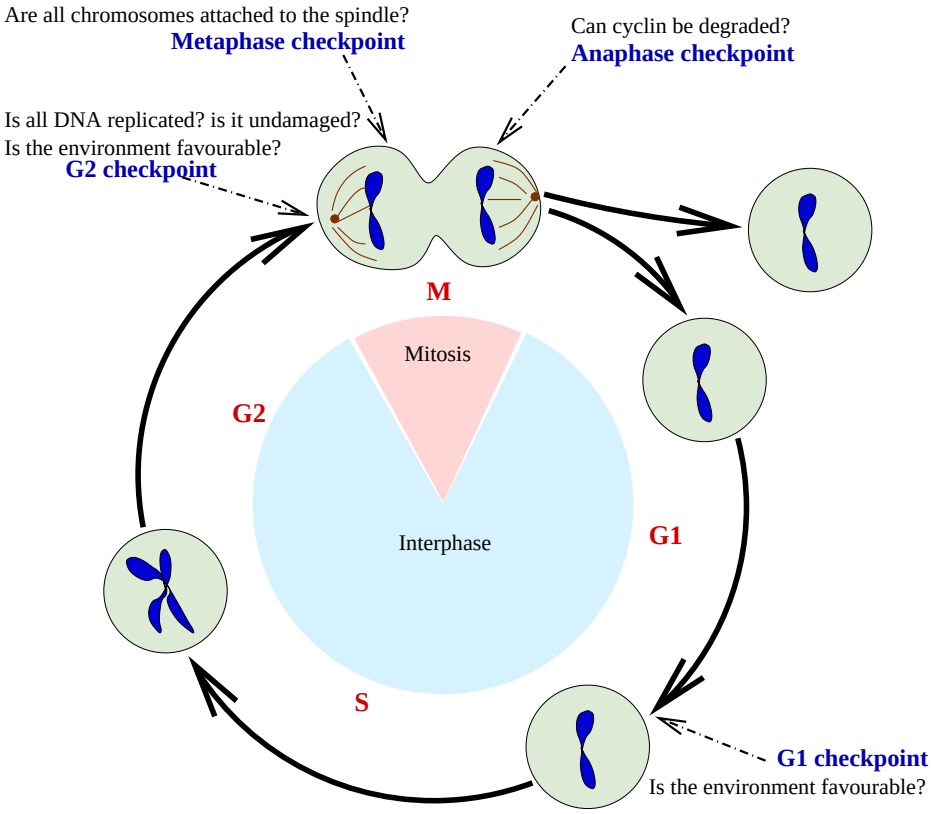

Figure 1.1: Phases and checkpoints of a typical cell cycle. Figure inspired by Lodish et al. (2003, Fig. 21-1).

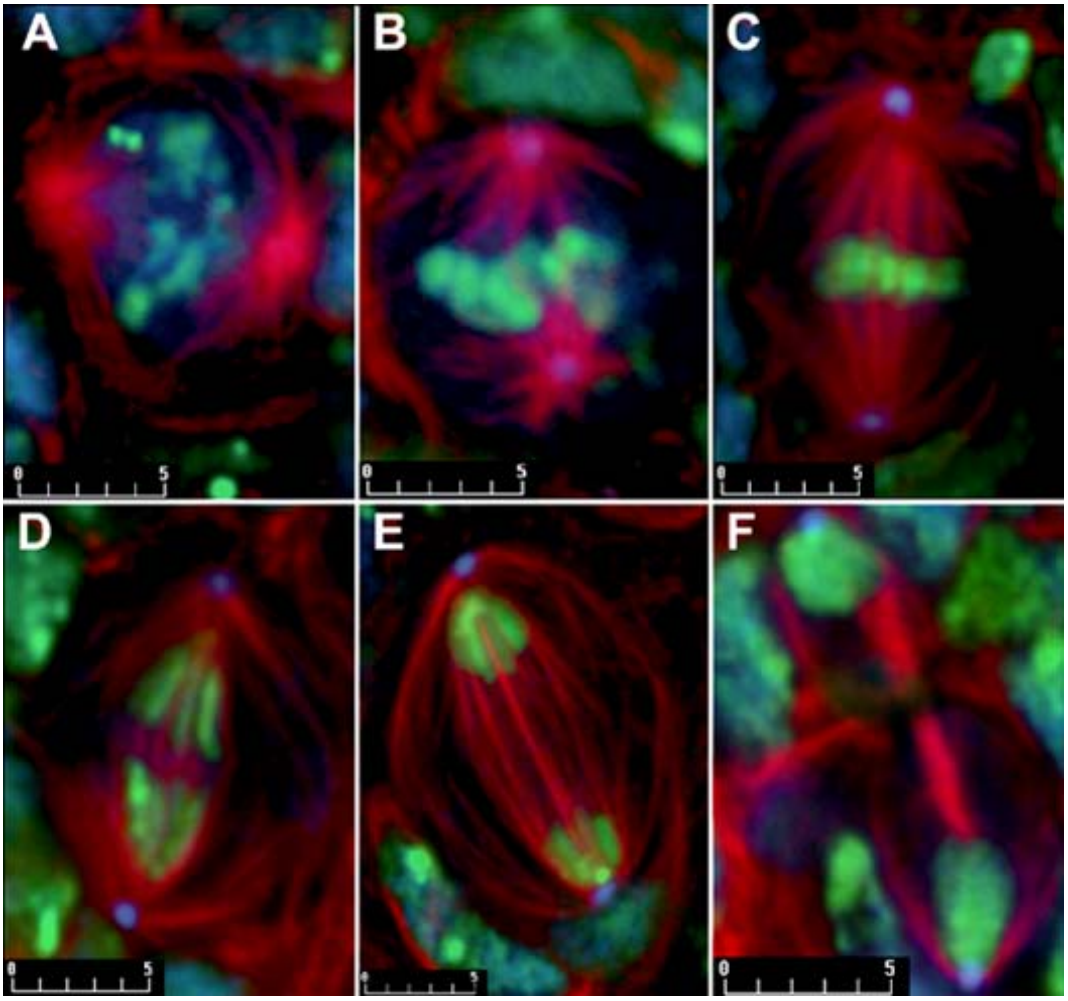

Figure 1.2: Events during mitosis in *Drosophila* cells as seen through a microscope. Color coding: Red - Tubulin (component molecules that are part of microtubules); Green - DNA. (A) Microtubule formation and chromosome condensation; (C) Chromosome pairs lined up for separation; (D,E) Chromosome separation. Compare with Fig.[1.3]. *Courtesy*: Wojcik lab, Virginia Tech.

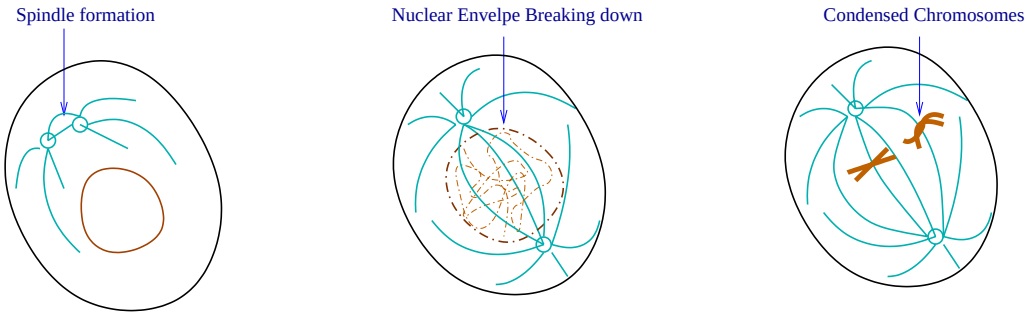

Figure 1.3: Events during mitosis - a schematic. Compare with Fig.[1.2].

regulators of the cell cycle. For instance, active Cdk1-cyclin B complex (also called MPF) is the main promoter of early mitotic events. Without the cyclin subunit, the CDK subunit is inactive. Phosphorylation of the CDK subunit at specific activating and inactivating sites also regulates its activity. Because we focus on entry into mitosis and how it is affected by unreplicated DNA, we focus on MPF and its regulation.

From interphase to mitosis, MPF undergoes many regulatory steps. Although the amount of Cdk1 is constant throughout the cell cycle, cyclin B is absent on entering interphase and needs to be synthesized from its mRNA template. Cyclin B rapidly combines with the Cdk1. This dimer of Cdk1 and Cyclin B can be activated by phosphorylation on Thr-161 and inactivated by phosphorylation on Thr-14 and Tyr-15. During interphase, the activating phosphorylation on Thr-161 is rapid and has a half-life of 1 min (Kumagai and Dunphy, 1995, Fig. 5B). We do not know of evidence suggesting regulation of the Thr-161 phosphorylation during cell cycle (i.e., it is considered a constant activity). The inactivating phosphorylations of MPF, however, are regulated by MPF itself. Wee1 acts as an inactivating kinase on MPF phosphorylating it on Tyr-15. Myt1 is another MPF inactivating kinase that phosphorylates MPF on both Tyr15 and Thr-14. Cdc25 is a dual specificity phosphatase that removes these phosphate groups and activates MPF. By acting as a kinase on these regulators, MPF inactivates Wee1 (Mueller et al., 1995a) and Myt (Mueller et al., 1995b) and activates Cdc25 (Izumi and Maller, 1993), leading to two positive feedback loops. During interphase, Wee1 and Myt1 are active and MPF, though phosphorylated on Thr-161, exists mostly in inactive form due to Tyr-15 phosphorylation. An increase in total MPF (due to increasing cyclin) increases the amount of active MPF. The feedback loops then cause a sudden drop in the activity of Wee1/Myt and activation of Cdc25 leading to abrupt MPF activation (Solomon et al., 1990). MPF is also known to regulate its own inactivation by promoting the destruction of its Cyclin B subunit. This happens during anaphase while exiting mitosis. Since we are concerned with delay in entry into mitosis, we deal only with the positive feedback loops.

Active MPF is the key promoter of early mitotic events. Activated MPF phosphorylates several substrates including nuclear lamins, microtubule binding proteins, condensins, and Golgi matrix components. These events are important for nuclear envelope breakdown, centrosome separation, spindle assembly, chromosome condensation, and Golgi fragmentation respectively (reviewed in

Nigg (2001)). Furthermore, MPF also activates anaphase promoting complex (APC) which leads to cyclin-B degradation that causes the inactivation of MPF leading to exit from mitosis (Nigg, 2001).

The two positive feedback loops due to MPF's regulation of its activator Cdc25 and inhibitors Wee1 and Myt1 (reviewed in Lew and Kornbluth, 1996) leads to the bistable nature of cell cycle (Sha et al., 2003; Pomerening et al., 2003). Our modeling considers this bistable nature as central to the cell cycle (see section [1.3.3] for details.). Thus, MPF activation (entry into mitosis) implies activation of Cdc25 and inactivation of Wee1 and Myt1, and vice-versa. Proteins that are activated by checkpoint signals, like Chk1, act on Wee1 and Cdc25, thus inhibiting/delaying these positive feedback loops (and hence entry into mitosis) in the presence of unreplicated DNA (henceforth UR-DNA). This is how the cell's response is modeled here.

Given the central role of DNA in cellular processes, it is plausible that the processes for its replication and distribution (to progeny) to have evolved into a robust mechanism capable of resisting many errors. **Checkpoints** are such mechanisms. They ensure progression to the next step upon the successful completion of previous one(s) (Hartwell and Weinert, 1989). For instance, the checkpoint for UR-DNA ensures that all chromosomes have been replicated before proceeding with their distribution to progeny by mitosis (Fig.[1.1]). The model presented here focuses on this checkpoint in cell cycle of frog egg extracts, an *in-vitro* system derived from frog eggs that is convenient for biochemical studies. Novak et al. (2002) has basic information about the cell cycle and provides a review of the different checkpoints in the cell cycle of various eukaryotes.

1.2 Why study these checkpoints?

Cancer cells have defects in regulating their cell cycle. The cell cycle of non-cancerous cells is regulated by various factors including growth (and anti-growth) signals, checkpoints, and apoptosis. Most cancer genotypes can be seen as a collection of physiological modifications that allow cells to forgo these inherent control mechanisms and invade and colonize surrounding tissue (Hanahan and Weinberg, 2000). Evading checkpoints may be one step towards cancer. For instance, this may lead to cells that have incorrectly replicated DNA and have mutations in genes crucial for inhibiting cell division in the presence of anti-growth signals. Understanding checkpoint mechanisms, like the UR-DNA checkpoint, will hopefully lead us closer to a solution for cancer. (Studying it in other organisms, like frog-eggs, makes sense because of the universal nature of cell cycle regulation.)

Historically, cancer has been characterized by mutations that produce oncogenes with dominant gain of function and tumor-suppressor genes with recessive loss of function. However, as more information about the components and complex pathways inside the cell is revealed, it appears that one needs to appreciate the workings of this complex 'wiring-diagram' of the cell to understand cancer (Hanahan and Weinberg, 2000, Fig. 2). Models like the one presented here are a step in that direction and may play a crucial role in such an understanding. This is, however, only a preliminary step and much more needs to be understood and included for a complete picture (For instance: heterotypic signaling between diverse cell types, the complex process of metastasis, etc. (Hanahan

and Weinberg, 2000).).

1.3 The experimental system and our current view

1.3.1 Frog eggs

Eggs of the South African clawed frog, *Xenopus laevis*, are convenient for investigations of the cell cycle because the initial cell cycles of the zygote proceed rapidly and synchronously. The ability to make cell-free extracts, which are easy to manipulate and do biochemical analysis, is a major advantage of this system over other eukaryotes like yeast. Like other amphibians, *Xenopus* embryos are large in size (diameter ≈1mm), develop outside the mother's body, and are available in large numbers. In addition, these frogs are easy to raise and can yield eggs throughout the year. (Elinson (2003) has introductory information on *Xenopus* as an experimental organism.)

Before treatment with progesterone, frog-egg cells, called immature oocytes, are arrested in the interphase of meiosis-I. After treatment with progesterone, they undergo meiosis-I and arrest in metaphase of meiosis-II of the second division. These mature oocytes can now fuse with the sperm (fertilization) to form a zygote. Fertilization triggers release from meiosis-II into interphase. The zygote then undergoes 12 rapid, synchronous cell cycles without the need for cell growth. This converts it into a hollow ball of 2^{12} (=4096) cells.

Microinjection (of mRNA and proteins) and manipulations of cell-free extracts are the main methods of studying the cell cycle in these embryos. The latter is the experimental system modeled in this study and is described briefly in the next section.

1.3.2 Cell-free egg extracts

Cell-free extracts derived from frog eggs are *in-vitro* experimental models of the *in-vivo* cell cycle. They are prepared by crushing the eggs by centrifugation, the supernant being the cytoplasmic extract (with yolk, pigment, and organelles pelleted to the bottom). Various types of extracts can be prepared from eggs in different phases of cell cycle and treated with different additives. Cytoplasm from unfertilized egg extracts (mature oocytes) is used in the experiments we cite. The extracts are arrested in the M-phase of the cell cycle. Addition of Ca^{++} mimics fertilization and releases the extract into interphase. These extracts then replicate DNA (if added, usually as sperm nuclei) and return to M-phase. Sperm nuclei are usually added to monitor the progression through cell cycle in these extracts. Condensed chromosomes and nuclear envelope breakdown imply M-phase (see Fig.[1.4]). Biochemical studies of MPF activity in these extracts is, however, the most accurate indicator of cell cycle state. Note that since transcription is not active in early frog-egg cell cycles, removal of the DNA does not hinder the cell cycle. Dasso and Newport (1990, Fig. 3) showed the lengthening of the S-phase when different concentrations of sperm nuclei were added to frog extracts in the presence of DNA replication inhibitor aphidicolin. This has become the common method of inducing the UR-DNA checkpoint. In the experiments cited (later) and used in making this model, the extracts for UR-DNA checkpoint have been supplemented with 1,000 sperm nuclei/μl and 100 μg/ml of aphidicolin.

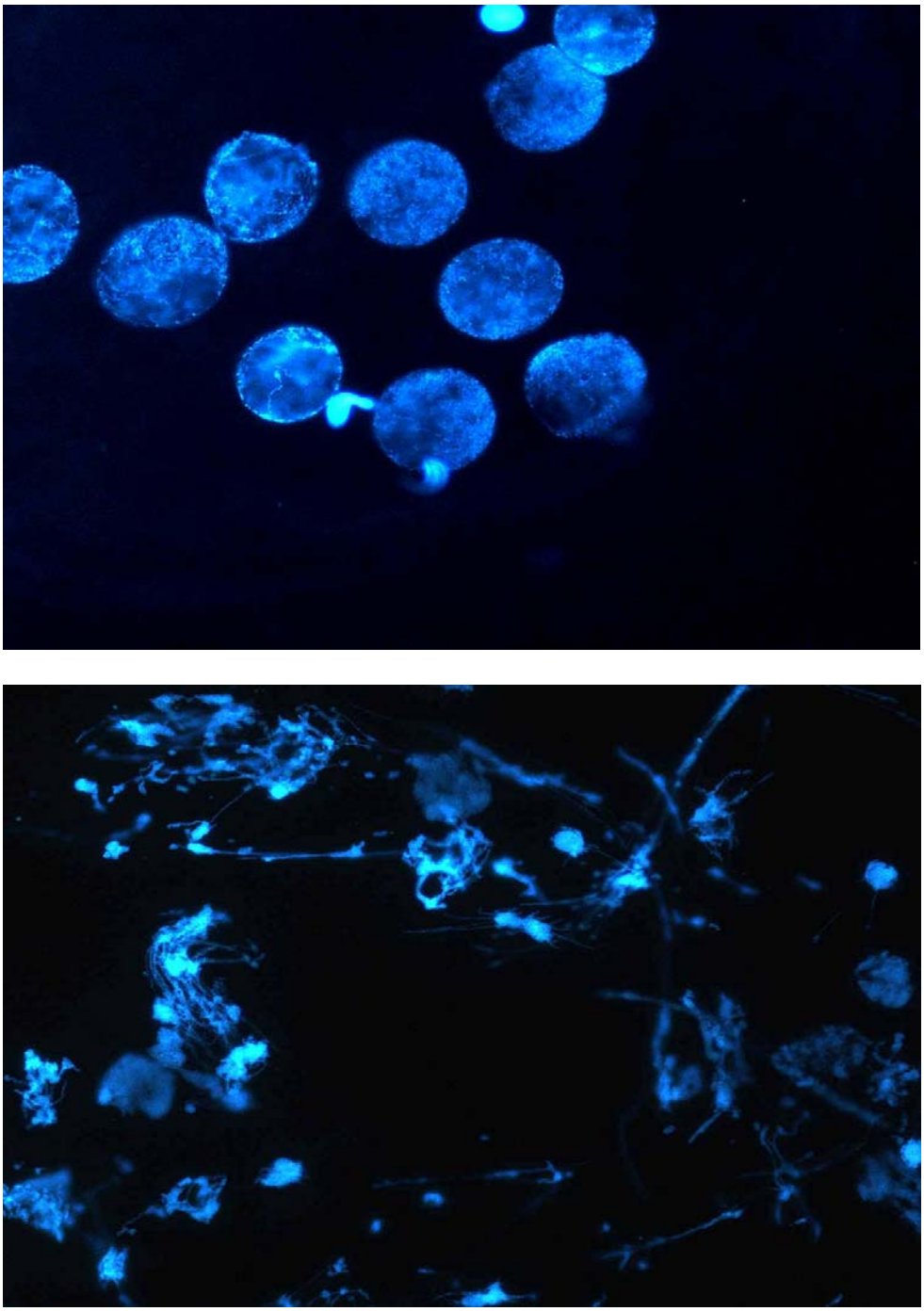

Figure 1.4: Events of cell cycle in frog-egg extracts. Top: Interphase, with intact nuclear envelopes; bottom: Mitosis, with broken nuclear envelopes. Compare with Fig.[1.2] on page 3.*Courtesy*: Sible lab, Virginia Tech.

Use of cytoplasm from a large number of cells allows biochemical analysis of the extract. We can regulate protein synthesis by addition of external mRNA or using a translation inhibitor (like cycloheximide). Proteins can also be added or depleted (using antibodies). The extract system has thus lead to many discoveries about the biochemistry of the cell cycle, even though it differs in some (important) ways from the *in-vivo* system (In intact cells, for instance, nuclei create compartments that are absent in the extracts).

1.3.3 Novak-Tyson model with unreplicated DNA

Previously, Novak and Tyson created a mathematical model for the cell cycle in frog-egg extracts (Novak and Tyson, 1993). The part of their 'wiring-diagram' that concerns us is shown in figure [1.6]. Their main proposal was that the MPF activation (through Cdc25 phosphatase) and inactivation (through Wee1 kinase) are abrupt transitions over a hysteresis loop (see Fig.[1.5]). (In the description below, MPF is the name of a molecule consisting of a dimer of Cdk1 and an M-phase cyclin, [MPF] is a variable referring to concentration of active MPF, and C_X is a constant with C standing for "total cyclin" (i.e., [cyclin]). 'C' is used since the related experiments are done using non-degradable cyclin which rapidly binds to Cdk1 forming inactive MPF.) In this figure, for $C_I <$ [MPF] $< C_A$, there are two stable steady-states separated by an unstable steady state. As [MPF] approaches C_A from below, the unstable and lower stable steady-state coalesce and vanish (at a saddle-node bifurcation) leaving only the 'high-MPF' stable steady-state for [MPF] $> C_A$. This simulates the transition from interphase (low MPF activity) into mitosis (high MPF activity). During exit from mitosis by degradation of cyclin proteins, [MPF] follows the 'high-MPF' steady-state until it abruptly jumps down after [MPF] $< C_I$ at the other saddle-node bifurcation. This diagram thus signifies the bistable nature of the cell cycle according to Novak and Tyson (1993).

Based on Fig.[1.5], Novak and Tyson (1993) also concluded that: (1) for $C_{total} = C_A + \epsilon$, the time-lag will increase abruptly as $\epsilon \to 0$; and (2) there will be a different threshold for MPF inactivation for extracts going from mitosis into interphase (at C_I).

The theoretical picture of transition from interphase into mitosis proposed by Novak and Tyson (1993) is consistent with the experiments of Solomon et al. (1990). When these experimentalists added exogenous (non-degradable) cyclin to interphase extracts with no endogenous cyclin, they found that activation of MPF required a critical threshold amount of cyclin, that the activation was abrupt, and that the amount of MPF activity generated increased with increasing exogenous cyclin. The other two predictions agree with the experiments done by Jonathan Moore (that were never published). This data is compared with the output of our new model (which is also bistable) in Fig.[4.4]. The inactivation threshold is measured by supplementing a mitotic extract with some amount of non-degradable cyclin (we call this amount C_{nd}; subscript 'nd' stands for non-degradable). As the degradable cyclin gets degraded, [MPF] tends towards its lower value during interphase. However, it is found that C_{nd} needs to be below C_I (with $C_I < C_A$) for the extract to enter interphase (low MPF activity). This value, C_I, is found by reducing the amount of C_{nd} until the transition into interphase (low MPF activity) is possible. The bistable nature of the cell cycle in the extracts of frog-eggs has been recently reconfirmed by Sha et al. (2003); Pomerening et al. (2003). Sha et al. (2003) also confirmed the model predictions about variation of lag time for entry into mitosis, and differing cyclin thresholds for activation and inactivation (refer previous

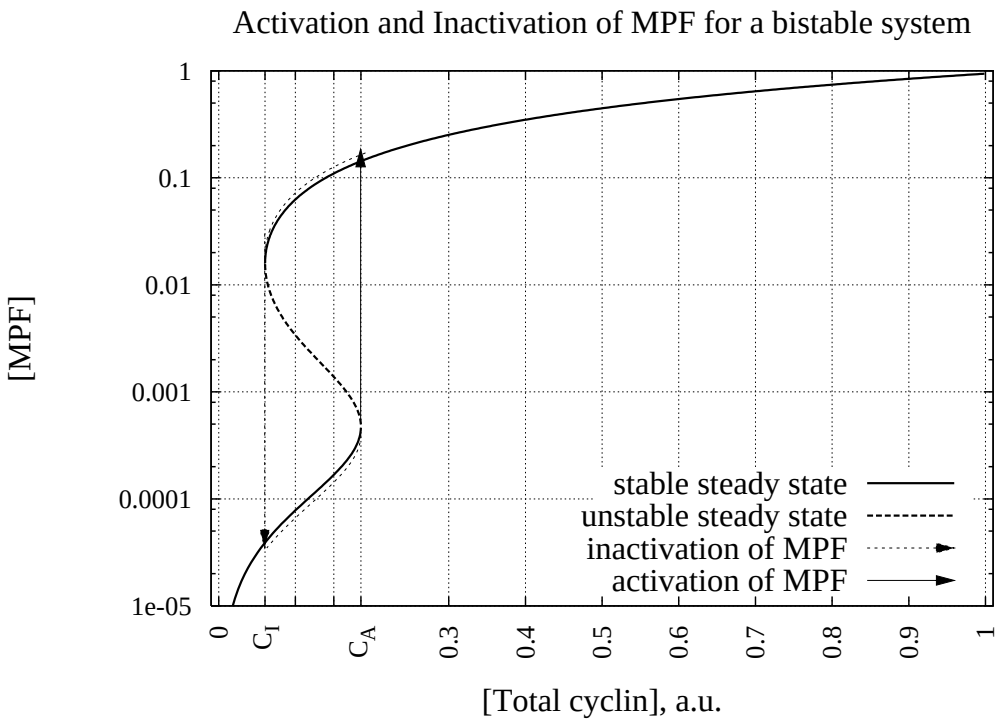

Figure 1.5: Bistable dynamics of the cell cycle. MPF is inactive (or low) during interphase and increases until [MPF] $> C_A$. It then activates, jumping to the 'high-MPF' steady state (Mitosis). Degradation of cyclin B leads to its inactivation - it follows the 'high-MPF' steady state until [MPF] $< C_I$, where it falls to the 'low-MPF' steady-state (Interphase). Since cyclin binds rapidly to MPF, and its availability limits the amount of MPF, the label on the horizontal axis could also be called 'Total MPF' instead of 'Total cyclin'.

paragraph). However, the model does not contain many newly discovered components. Our model incorporates these components while retaining the bistable picture.

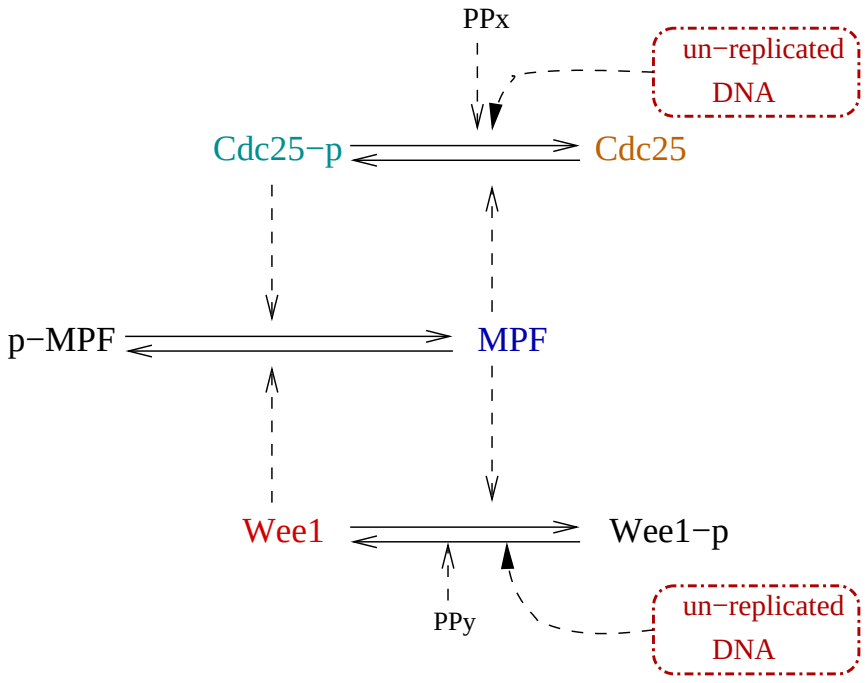

Figure 1.6: Effect of unreplicated DNA on MPF dynamics (based on Fig. 1(B) in Novak and Tyson (1993)). Compare with Fig.[2.4]. p-MPF stands for the phosphorylated (on Thr-14, Tyr-15) form of MPF that is inactive. [p-MPF] + [MPF] = Tm, where [p-MPF] and [MPF] are variables denoting the concentration of those species while Tm is a constant.

According to Novak and Tyson (1993), the UR-DNA checkpoint works by increasing the rate constants for keeping the MPF activator Cdc25 inactive and MPF deactivator Wee1 active. This leads to increasing the activation threshold on the hysteresis curve (lower saddle-node in Fig. [1.5] moves to the right). This higher active MPF requirement in presence of UR-DNA leads to a delay (or complete inhibition) in entering mitosis. We show that recent experimental evidence supports their basic idea (Sha et al., 2003).

In Chapter [2] we incorporate new experimental details into our wiring diagram. Then, in Chapter [3], we propose a hypothesis on how this checkpoint works. In the same chapter, after checking the rationale of this hypothesis, we incorporate it into our equations, thus making our model. Finally, we compare simulations of the model with experiments and come up with suitable parameter values in Chapter [4]. (Creation of the wiring diagram, hypothesis, mathematical model, and testing the model were not successive sequential processes as may appear from the sequence of chapters. The next section gives the actual steps that were followed.)

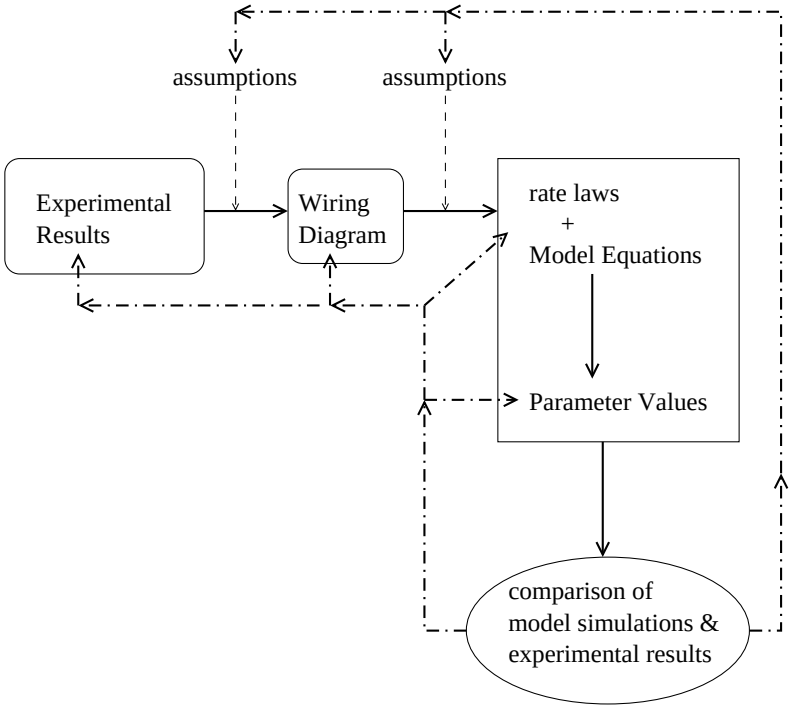

Figure 1.7: Process followed for making the model.

1.4 Model making

Figure [1.7] shows our approach to model making. We started by creating a detailed wiring diagram of our system (similar to Fig.[2.4], but without Myt1). Though more detailed than Novak and Tyson (1993), the new data used in the diagram agreed with the hypothesis (of Novak and Tyson (1993)) that the UR-DNA checkpoint operated by activating Wee1 and inactivating Cdc25. (Much of the information presented below is an outline of the details presented in Appendix [A] on page 43.)

Unlike the model of Novak and Tyson (1993) that uses Michaelis-Menten rate-law based switches (for Cdc25 and Wee1), we started making the model using only mass action kinetics. The Michaelian assumption applies when the amount of enzyme $\ll$ substrate. This breaks down in the feedback loops of Cdc25 and MPF, and of Wee1/Myt1 and MPF where each acts as an enzyme to the other (and hence the inequality is not true). Avoiding this and using mass-action based kinetics makes the model self-consistent. We assumed that the bistable nature of this system is a fundamental (invariant) property of the model. (Section [1.3.3] mentions experimental evidence that supports this.) Our starting goal was to get this bistable characteristic using a simple three variable model of the cell cycle of frog-egg extracts. This simple model was based on the old data that was available to Novak and Tyson (1993) (see Fig.[1.6]).

The first problem was to know if this simpler model would give the bistable characteristic. We

used the program called Chemical Reaction Network Toolbox (CRNT) for this purpose (Feinberg and Ellison, 1999). For the given reaction network, this program told us that multiple steady states were possible and gave us a sample parameter set for which this would happen. With a minor modification of this model, we were able to retrieve the bistable nature (see section A.1 in Appendix [A] for details).

To get a parameter set that accounts well for the data suitable for the simpler model, we fed this bistable model into the parameter optimizer developed in the Tyson lab (Zwolak et al., 2004a,b). We then created the updated (newer) model from our new wiring diagram. The optimized parameters gave us starting values for parts of the newer model. We used them in the newer model and attempted to guesstimate the remaining parameters 'by hand'. The range integration function in the XPPAUT program was our primary tool. This allows one to see how the simulation results were affected as we stepped through one or two parameters (in a specified range). Newer experimental data on the effect of Wee1 depletion and mutant forms of Cdc25 on nuclear envelope breakdown (NEB) was used for this purpose. We discovered during this process that accounting for the same NEB timing in the absence of Wee1 would require another kinase acting on MPF. Based on the experimental literature, Myt1 appeared the most suitable choice (Mueller et al., 1995b). Including Myt1 meant updating our wiring diagram and re-parameterizing the model. Fortunately, it did not take much parameter twiddling to fit sufficient number of available experiments.

Equations [3.1 – 3.13] on page 23 are the resulting equations of this latest model; Table [3.1] has the basal parameter values, and table [3.2] gives the initial conditions. Figures [4.2 – 4.6] starting page 33 compare model simulations and the data from the literature.

Chapter 2

From experimental information to the wiring diagram

2.1 Review of experimental information about the system

We first take an overview of the concept of checkpoints and how it has evolved with our increasing knowledge of cellular processes. Then, we take a more detailed look at the workings of the unreplicated DNA (UR-DNA) checkpoint.

2.1.1 The unreplicated DNA checkpoint

The cell cycle is a cyclic sequence of events, each of which depends on the successful completion on previous event(s). Blocking or perturbing a specific event reveals these interdependencies. Hartwell and Weinert (1989) defined checkpoints as mechanisms extrinsic to the successful completion of an event of cell cycle that drive the next event. It is, however, becoming clear that checkpoints are not simple isolated modules, but are highly integrated parts of the cell physiology (Zhou and Elledge, 2000). For instance, the cell's response to DNA damage (including UR-DNA) may include delay in cell cycle transition, apoptosis, control of replication, and activation of DNA repair mechanisms (Fig.[2.1]). The cell's response to DNA damage or UR-DNA can be viewed as the work of a network of interacting pathways of signals, sensors, transducers, and effectors. Checkpoints constitute those parts of the pathway that relate directly to progress of cell cycle. This broader definition is necessary because of our growing knowledge of the complexity of this process (Zhou and Elledge, 2000). However, this conceptualization of the pathways into sensors, etc. is our attempt to understand cell cycle regulation – such clear-cut "engineering-like" demarcation of function is not honored by the cell (Sancar et al., 2004). Describing or reviewing all the information relating to the cell's response to UR-DNA thus seems impracticable. We attempt to give an outline of the cells response and then describe just the checkpoint related pathways.

Fig. [2.1] shows an outline of the cell's response to DNA damage and unreplicated DNA. This picture is generic and true for most eukaryotes. We will deal with the components (mostly) exclusive

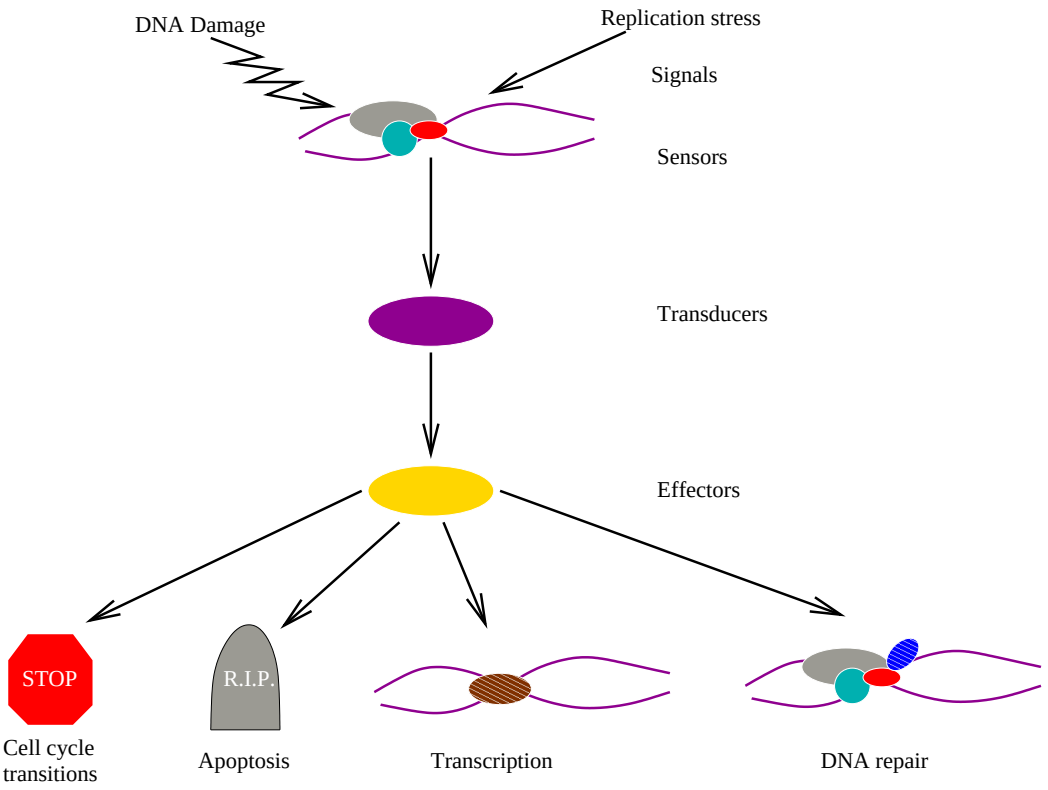

Figure 2.1: A contemporary view of the general outline of the signaling pathway activated by damaged or unreplicated DNA. Based on Zhou and Elledge (2000, Fig. 1).

to cell cycle delay/halt. Dasso and Newport (1990) showed that the presence of a threshold level of unreplicated DNA in the extracts of frog-eggs causes the cell cycle to halt before mitosis. They showed that this inhibition was caused by blocking the activation of MPF. This block in activation was not due to the regulation of cyclin synthesis or the dimerization of cyclin and Cdk1.

Many molecules taking part in the cellular response to UR-DNA have been recognized. Since the picture is similar in all eukaryotes, it is usual in the literature to reference various model systems (humans, yeast, frog eggs, etc.) to get an overall description of the molecular control system. For the cellular response to UR-DNA signal, one could term ATR as the sensor, Chk1 the transducer and Cdc25 and Wee1 the effector proteins. Fig.[2.2] shows these components.

ATR is a serine-threonine protein kinase required in the cellular response to UR-DNA (Guo et al., 2000). It is a member of a family of large proteins (275-500 kDa) with a unique protein kinase domain at their C termini (Nyberg et al., 2002). The Chk1 protein, especially the nuclear fraction, is phosphorylated in the presence of UR-DNA (Kumagai et al., 1998a, Fig. 6A). Depletion of ATR abrogates the phosphorylation of Chk1 in the presence of UR-DNA (Guo et al., 2000, Fig. 3B). ATR is thus a known activator of Chk1 in the presence of UR-DNA.

It has been proposed that Chk1 acts on the cell cycle engine to keep MPF in its inactive form

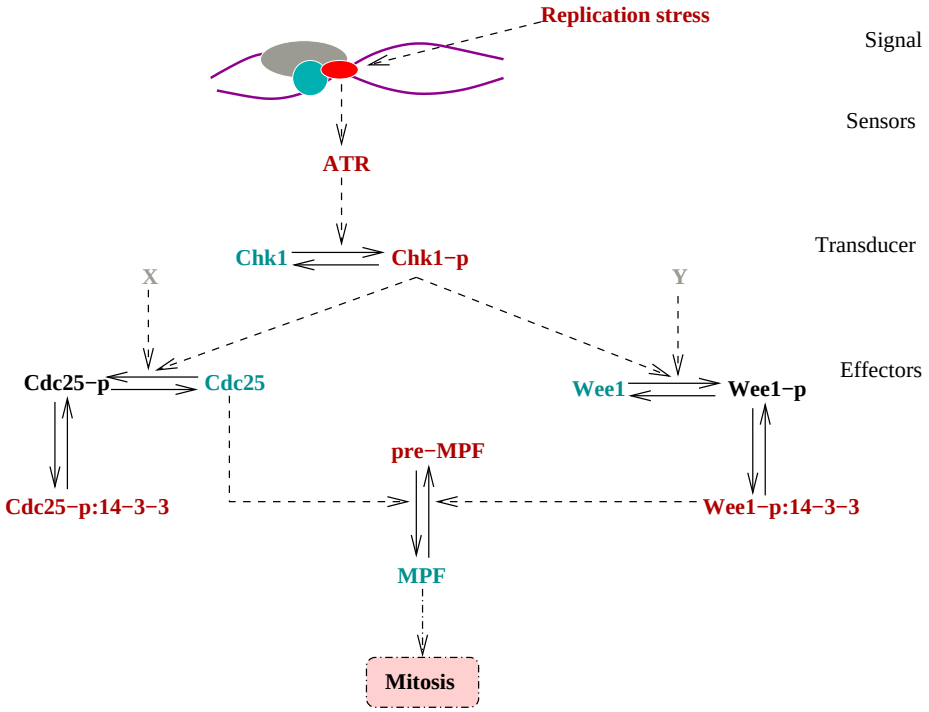

Figure 2.2: A general outline of the UR-DNA signaling pathway in frog egg extracts. Compare with Fig.[1.6].

by maintaining its Tyr-15 phosphorylation. Chk1 is supposed to do this by inactivating Cdc25 (Kumagai et al., 1998b,a), the MPF activating phosphatase, and activating Wee1 (Lee et al., 2001), the MPF inactivating kinase. The regulation of Cdc25 and Wee1 also involves their association with the protein 14-3-3. Kumagai et al. (1998a) showed that Chk1 is highly phosphorylated in the presence of UR-DNA. They also show that recombinant Chk1 phosphorylates recombinant Cdc25 on Ser-287 *in-vitro*, and that this phosphorylation confers the Cdc25 with ability to bind recombinant 14-3-3 protein. They showed that immunodepletion of Chk1 from extracts advanced the NEB by about 20 minutes (see Fig. 3B), thus indicating the importance of Chk1 in the timing of even an unperturbed cell cycle. Further, in the presence of UR-DNA, depletion of Chk1 partially abrogates the delay/block in the NEB (see Fig. 3C).

Earlier, Kumagai et al. (1998b) showed 14-3-3 to be a negative regulator of Cdc25. According to this article, Cdc25 is bound to 14-3-3 only during interphase and not mitosis. This binding is mediated by the phosphorylation of Cdc25 on Ser-287. Abolishing this phosphorylation by a point mutation (replacing serine with alanine) leads to advance in NEB of the normal cell cycle and partial abrogation of checkpoint-induced delay in the presence of UR-DNA. Kumagai et al. (1998a) showed (see Fig. 4B) that though Chk1 confers Cdc25 the ability to bind 14-3-3, depletion of Chk1 does not affect the binding of Cdc25 to 14-3-3 significantly. This indicates the presence of some additional and perhaps more significant mechanism leading to this binding; it may either

be another kinase or an entirely distinct mechanism[1]. However, the catalytic activity of Cdc25 against Cdk1 is not significantly different for the WT (wild type) and S287A[2] form (that cannot bind 14-3-3). This led to investigation of 14-3-3 mediated regulation of Cdc25 by other means. Kumagai and Dunphy (1999) showed that in Xenopus tissue culture cells, a mutated Cdc25C that cannot bind 14-3-3 is mainly nuclear, while the WT Cdc25C is mainly cytoplasmic. Margolis et al. (2003) have shown that 14-3-3 is removed from Cdc25 before dephosphorylation of Ser-287. This implies that the step of 14-3-3 removal and its regulation may be crucial to Cdc25 activation. (We hope this will be clarified by future experiments).

There are three known isoforms of Cdc25 in vertebrates - Cdc25A, Cdc25B, and Cdc25C. For the UR-DNA checkpoint, we are mainly concerned with the C and A forms (Uto et al., 2004). (In the above discussion, Cdc25 meant Cdc25C.) Bulavin et al. (2003b,a) have shown that the phosphorylation of Cdc25C on Ser-285 and Ser-287 are antagonistic – only one of these Ser can be phosphorylated at a time. Kumagai et al. (1998a) had already shown that Chk1 phosphorylates Cdc25C on Ser-287 meditating its binding to 14-3-3, and that most of Cdc25C is bound to 14-3-3 during interphase. This was interpreted by us into the Cdc25 portion of wiring diagram (Fig.[2.4]). New evidence from Uto et al. (2004) showed that it indeed was the phosphorylation of Cdc25 proteins (A and C) by Chk1 that blocked interaction with Cdk1-cyclin B (MPF). However, Cdc25A appears to be a significant component of the checkpoint mechanisms. (We have not considered Cdc25A because of lack of sufficient data until recently.)

Only one article (Lee et al., 2001) dealt with the UR-DNA checkpoint acting through Chk1's action on Wee1. They have suggested that Wee1 is positively regulated by Chk1 and 14-3-3 proteins, though unlike Cdc25, no mutually exclusive phosphorylated forms of Wee1 are known or predicted based on analysis of its amino-acid sequence. Thus, a fraction of Wee1 is seen to be 14-3-3 bound during interphase, this form being the most active form of Wee1 (according to in-vitro kinase activities against MPF). 14-3-3 binding also conferred it an even distribution throughout the nucleus in Xenopus tissue culture cells (Lee et al., 2001, Fig. 3). This combination of binding to 14-3-3 and localization presumably make it the most potent form of Wee1. Chk1 (and at least one other kinase) was shown to phosphorylate Ser-549 on Wee1, this being a requirement for Wee1:14-3-3 binding. A look at our wiring diagram in Fig. [2.4] shows how these facts (and assumptions) were incorporated. However, the hypothesis that Wee1 is activated by Chk1 and 14-3-3 during the UR-DNA checkpoint is debatable. Lee et al. (2001) themselves point these out in the discussion section (pg. 561) saying, *"Immunodepletion of Chk1 does not abolish 14-3-3 binding to Wee1... we have not been able to detect an increase in kinase activity or binding of 14-3-3 proteins in the case of Xwee1 that has been immunoprecipitated from aphidicolin-treated extracts... only a small fraction of Xwee1 is associated with 14-3-3 proteins in egg extracts... these considerations suggest that there may be technical limitations in how Xwee1 can be assayed in checkpoint-activated extracts."* Our wiring diagram for the Wee1 portion is thus much more hypothetical than for the Cdc25 portion.

Unlike Wee1 which phosphorylates Tyr-15, Myt1 is a membrane associated dual specificity kinase

[1] It should be noted that in these studies, typically one or two components of the perturbed system are monitored. The choice of these components, like Cdc25 and 14-3-3, is based on a hypothesis that emerges from the combined picture created using various model organisms (yeast, humans, etc.). It is possible, however, that additional undiscovered interactions with other cell cycle proteins exist and are significant. One major goal of building our computational model is to predict such interactions.

[2] A mutant form of the protein with serine at amino-acid location 287 replaced by alanine.

that phosphorylates both Tyr-15 and Thr-14 (Mueller et al., 1995b). Myt1 is the major Cdk1 specific dual kinase, and is located in the membrane fraction of Xenopus egg extracts (Mueller et al., 1995b, Fig. 4). Also, Myt1 seems to be regulated during I and M phases, with about 5 times higher activity on Cdk1 during I phase. Its kinase activity towards Cdk1 does not seem affected by the presence of UR-DNA (Mueller et al., 1995b, Fig. 5). Our model has both Wee1 and Myt1 acting as kinases leading to MPF phosphorylation with only Wee1 affected by the presence of UR-DNA (see Fig.[2.4]).

The picture of the role of Chk1 in the UR-DNA checkpoint is still fuzzy. Though depletion of Chk1 leads to cell cycle advance (Kumagai et al., 1998a, Fig. 3B), its depletion does not significantly affect Cdc25 and Wee1 phosphorylation and binding to 14-3-3. These facts are incorporated by the 'X' and 'Y' kinases acting in parallel to Chk1 in Fig. [2.2]. Uto et al. (2004) have recently shown in early frog embryos that Cdc25A is affected by Chk1 phosphorylation, making it incapable of interacting with Cdk1. However, it is unknown whether Cdc25A is present in extracts or not. Walworth (2001) reviews some of these issues in more detail. As we discuss later, this fuzziness has translated into some of the assumptions of the wiring diagram of our model.

2.1.2 Assumptions and our wiring diagram

Although the core of the Novak and Tyson (1993) wiring diagram holds true, new forms of Cdc25 and Wee1 and new proteins Chk1 and 14-3-3 have been added to it (compare Fig.[1.6] and Fig.[2.4]). In the previous section, we described this data for the components in the new wiring diagram. Some generic and specific assumptions were made due to lack of sufficient data and to simplify the wiring diagram. In all cases, our hope is that understanding of a simplified model will become a step towards a complete understanding later. Below are the generic assumptions:

- Phosphatase activity is not regulated. Though initially regarded as constitutively active enzymes, protein phosphatases appear to have sophisticated regulatory mechanisms (Hunter, 2000). These details are not definitely known for phosphatases that seem to be involved in the cell cycle. Our model is phenomenological[3] and we proceed by assuming that the unknowns are insignificant to the problem.

- Effects of nuclear localization of components is ignored. These effects appear to be significant in Wee1 (Lee et al., 2001) and Cdc25 (Kumagai and Dunphy, 1999) regulation through their binding to 14-3-3 proteins. The localization effects may become important when the extracts are supplemented with sperm nuclei for monitoring the phase of the cell cycle.

For convenience in dealing with specific assumptions, we divide the wiring diagram into three subsystems:

[3]reproduces the main characteristics of the phenomena using the well known components that interact in a simplified manner

MPF subsystem

As described in the introductory section, MPF is considered the key regulator of the cell cycle. When active, it leads to characteristic events of mitosis.

This part of the system was modeled using two forms of MPF: active and inactive (phosphorylated). Novak and Tyson (1993) used four forms because they consider both the activating (Thr-161) and inactivating phosphorylation (Thr-14, Tyr-15) of MPF (see section [1.1] for details). It is known that newly formed cyclin binds Cdk1 within 5 minutes (Solomon et al., 1990), and this dimer, MPF, gets phosphorylated on Thr-161 with a half life of 1 min (Kumagai and Dunphy, 1995). The latter step is not known to be regulated (reviewed in Kaldis, 1999) and was felt unimportant to the focus of this model. Hence, in our model, cyclin synthesis is assumed to lead directly to MPF formation ($k1$). During interphase, the high activity of Wee1/Myt1 and low activity of Cdc25 means this forms gets quickly inactivated by phosphorylation.

Cdc25 subsystem

Our model incorporates only one isoform of Cdc25. The wiring diagram is based on the mutually exclusive phosphorylations of Cdc25C on Ser-285 (active form) and Ser-287 (inactive form). The Cdc25A form appears to be significant to the UR-DNA checkpoint. Uto et al. (2004) have shown that its phosphorylation by Chk1 makes it unable to act on Cdk1-cyclin B. This form, however, does not have the regulation through Ser-287/Ser-285 (Bulavin et al., 2003a,b), and unlike Cdc25C, its total amount is known to fluctuate through the cell cycle of embryos. However, the presence of Cdc25A in extracts still needs verification. Hence our model does not incorporate Cdc25A.

Wee1 subsystem

In the article by Lee et al. (2001), we have some evidence suggesting that Chk1 activates Wee1 by phosphorylating it on Ser-549 that causes it to bind 14-3-3. Based on these suggestions, we hypothesized that Wee1 exists in four inter-convertible forms based on phosphorylations either by Chk1, causing the binding to 14-3-3, or by MPF that inactivates it. We take only the forms not phosphorylated by MPF to have a significant kinase activity against MPF.

Myt1 subsystem

Please see figure [2.3] taken from Lee et al. (2001, Fig. 5B). Note that the timing for 50% NEB is the same for the mock (ΔMock) and Wee1 (ΔXwee1) depletions, thus implying that Wee1 is insignificant for mitotic entry during the normal cell cycle. However, in the presence of UR-DNA, Wee1 depletion (ΔXwee1+APH) differs from the mock depletion (ΔMock+APH). It therefore seems plausible that Myt1 is the most significant kinase that inactivates MPF during interphase (so that Wee1 depletion does not affect the timing by much). However, the activity of Wee1 becomes significant in the presence of UR-DNA (incorporated through β in our model). We thus take a linear combination of Myt1 and the active forms of Wee1 for the kinase activity against

MPF. These roles of Myt1 and Wee1 differ from the Novak and Tyson (1993) model of the system. Their model has a single kinase, Wee1, whose activity is increased in the presence of UR-DNA (see Fig.[1.6]).

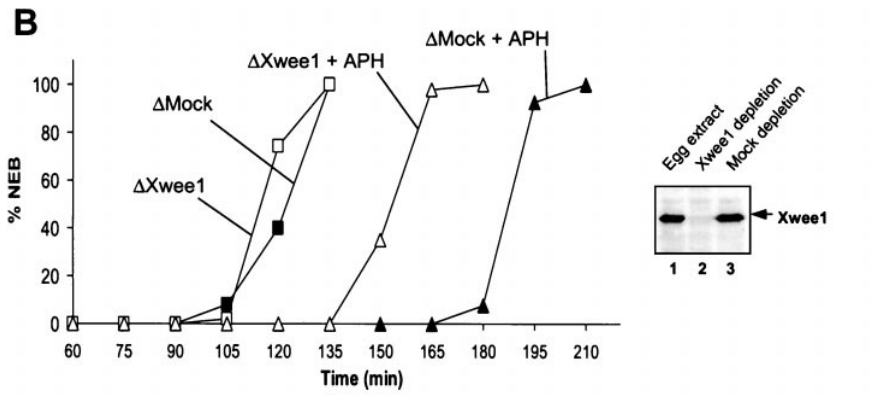

Figure 2.3: Example of %NEB data. *Source*: Lee et al. (2001, Fig. 5B) - requested for permission.

2.2 Wiring diagram: the current consensus

An overview of the experimental information and the assumptions that have led to the wiring diagram was given in the previous section. Below, we show the wiring diagram of our model and provide brief information about the interactions (labeled) in the wiring diagram (table [2.1]).

Following are the general references (review articles). CDKs and cell cycle control: Morgan (1997); Lew and Kornbluth (1996). Mechanisms of DNA repair and damage checkpoints: Sancar et al. (2004); Nyberg et al. (2002); Novak et al. (2002); Zhou and Elledge (2000).

Label		Reference/Notes
a	:	See Kumagai and Dunphy (1991, Fig. 2). Reviewed in Lew and Kornbluth (1996). Experiment in Kumagai and Dunphy (1995, Fig. 4B) was used in parameter estimation of $kc285$ and $rkc285$.
b	:	See Kumagai and Dunphy (1992); Izumi and Maller (1993); Bulavin et al. (2003b,a).
d	:	See Margolis et al. (2003); Kumagai et al. (1998b); Kumagai and Dunphy (1999).
c2, d	:	See Kumagai et al. (1998a,b); Kumagai and Dunphy (1999). Uto et al. (2004) show data on inhibition of Cdc25A through Chk1. Guo et al. (2000) show the requirement of ATR for phosphorylation of Chk1 in response to UR-DNA.
e	:	See Kumagai and Dunphy (1995, Fig. 4A). Reviewed in Lew and Kornbluth (1996).
e1, h	:	See Mueller et al. (1995b).
e2, g	:	See Lee et al. (2001); Mueller et al. (1995a).
f1, f2	:	See Mueller et al. (1995a). Some information in Lew and Kornbluth (1996).

Table 2.1: References used to make the wiring diagram.

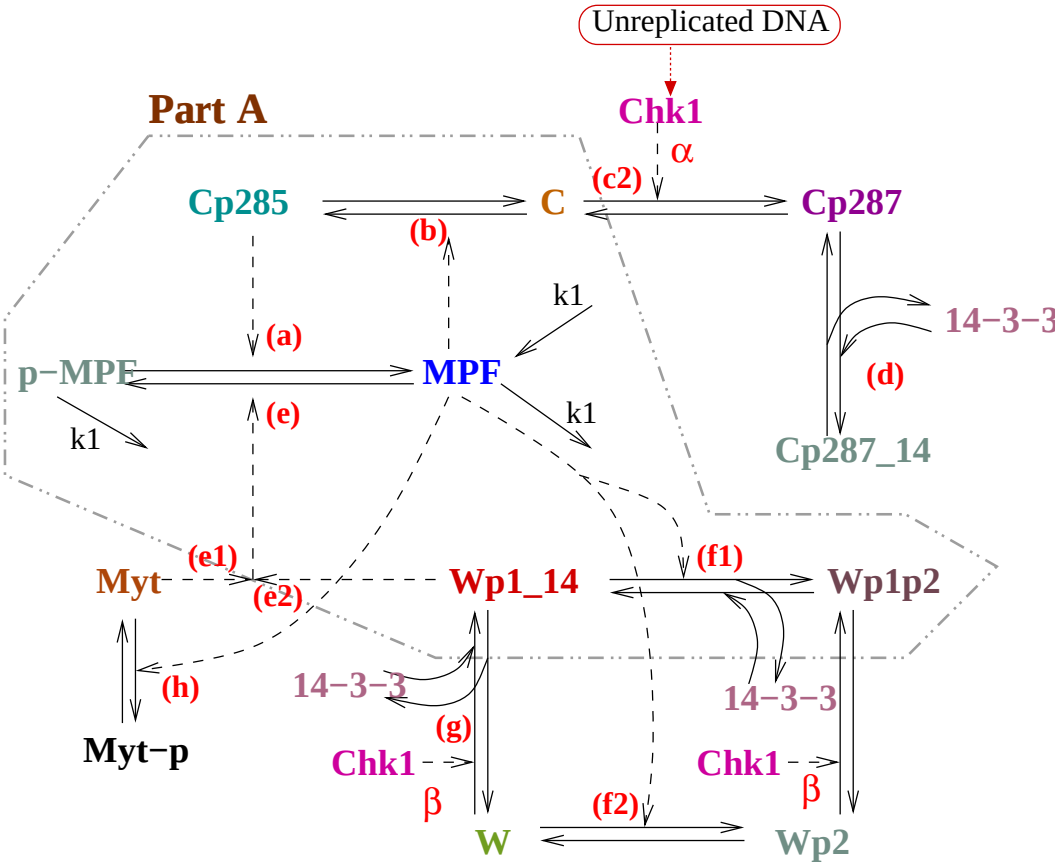

Figure 2.4: Wiring diagram of our model. p-MPF is the form of MPF that is inactivated by Tyr-15 and Thr-14 phosphorylation (though Thr-161 activating phosphorylation is present). In above figure, names starting with C and W refer to forms of Cdc25 and Wee1 proteins; the part after C/W starting with 'p' represents their phosphorylation state, and '_14' indicates binding with protein 14-3-3. Cp285 and Cp287 represent Cdc25 phosphorylated on amino acid number 285 and 287 respectively; Cp287_14 is Cp287 bound to protein 14-3-3. For W, phosphorylation by Chk1 at p1 enables its binding to 14-3-3 as depicted by Wp1_14; W is phosphorylated on p2 (in Wp2 and Wp1p2) and inactivated by MPF. α and β refer to the activities of the kinases Chk1, X, and Y in the UR-DNA pathway shown in Fig.[2.2]. Both α and β increase in the presence of UR-DNA. 'Part A' of this wiring diagram corresponds with the original Novak and Tyson (1993) model in Fig.[1.6] on page 10.

Chapter 3

From the wiring diagram to the model

Model making, as done here (Fig.[1.7]), involved going from the experimental information to the wiring diagram, and from there to the model equations. As indicated in Fig.[1.7], it was also an iterative process. Both these steps required us to make simplifying assumptions. For various reasons including: our lack of sufficient data for incorporating all elements; our incomplete understanding of complicated non-linear systems (as compared to the simpler ones) and our inability to assemble complicated pieces together 'by hand'. Please note the implicit assumption that this reductionist approach does not drastically hamper our understanding of the system and our ability to predict from it. We first list the main assumptions underlying our model, and then the ones made in the transition from the wiring diagram to the model equations. (The assumptions that are part of the wiring diagram were noted in the previous chapter.)

- The system can be treated as a well-stirred reactor (i.e., the concentrations of all species are same at every point in the system). This implies that we are justified in using ordinary differential equations (ODEs) to model the system.
- When sperm nuclei are introduced to monitor the phase of the cell cycle, their effect on the experimental system is insignificant and need not be considered in the model. The compartmentalization introduced by sperm nuclei and the additional components they bring to the extract may be significant.

Please note that this computational model is a model of the extract system, which itself is an experimental model for the intact cell.

3.1 Assumptions, rate laws, and model equations

We lack time-series (or kinetic) data on the new forms of Wee1 and Cdc25, and on 14-3-3 and Chk1. Hence, we need to guesstimate the rate constants. However, the steady state and %NEB data appear enough to model the checkpoint. We make the following (ref. Fig. [2.4] on page 21):

Hypothesis: During the unreplicated DNA checkpoint, the kinase activities of checkpoint proteins – Chk1 and other kinase(s) – towards their substrates are increased.

In the Cdc25 subsystem, for instance, this hypothesis implies that when the checkpoint is activated, the ratio $[Cp287]/[C]$ is higher. This, we suppose, keeps Cdc25 from being activated readily thus delaying the entry into mitosis. The same hypothesis applies, in general, to the Wee1 subsystem. The similarity of this idea to that of Novak and Tyson (1993) is apparent, but now experimental evidence backs these assumptions. We write down the model equations keeping this hypothesis in mind, and use them to analyze the Cdc25 subsystem to verify our hypothesis.

A look at the wiring diagram in Figure [2.4] and the model equations [3.1 – 3.13] makes the form of the equations clear. Each equation is of the form

$$x' = (\text{production terms}) - (\text{removal terms}),$$

implying that x is a *variable* in our model whose rate of change with time (the left side of previous equation) depends on interactions leading to its synthesis and degradation (the right hand side). Each synthesis and degradation term in the equation results from arrows (in the wiring diagram) pointing towards and away from x, respectively. Each of these interactions (arrows in wiring diagram) is characterized by variable molecular concentrations (substrates) and fixed *parameters* (rate constants). Thus the previous equation tells us the (instantaneous) rate of change of x depends on the (instantaneous) value of various variables and (fixed) parameters. (Variables are the symbols appearing on the left hand side of our equations; parameters are those symbols that are not variables.) Table [3.1] gives the value of model parameters. To know the value of all variables at any moment in time means that we know the 'state' of the system. For computing the state of our system at any moment, in addition to the rates of change of variables and the parameter values, we need the initial values of the variables. Table [3.2] gives these values.

Please refer the wiring diagram in Fig.[2.4] and its legend, and equations [3.1–3.13] for clarification of the notation. Note that we use a 'computer-science' notation for equations: variables and parameters in the equations are denoted by strings (rather than single symbols) with products denoted by a '$\cdot$'. For example, m =[MPF]; Tm =[MPF] + [p-MPF] = "total MPF".

- MPF subsystem

$$\begin{aligned} Tm' &= k1 - k1 \cdot Tm && (3.1)\\ m' &= k1 - k1 \cdot m + km \cdot \{(cp285 + rkmc) \cdot (Tm - m) \\ &\quad -rkm \cdot (aw \cdot wp1\_14 + am \cdot myt + rkmw) \cdot m\} && (3.2) \end{aligned}$$

- Cdc25 subsystem

$$
\begin{aligned}
cp285' &= kc285 \cdot \{(m \cdot c) - rkc285 \cdot cp285\} && (3.3)\\
cp287' &= kc287 \cdot \{-cp287 + (\alpha \cdot c)\} \\
&\quad -kc287\_14 \cdot \{-cp287\_14 + (\omega \cdot cp287)\} && (3.4)\\
cp287\_14' &= kc287\_14 \cdot \{-cp287\_14 + (\omega \cdot cp287)\} && (3.5)
\end{aligned}
$$

- Wee1 (and Myt1) subsystem

$$
\begin{aligned}
wp1\_14' &= kw\_mpf \cdot \{wp1p2 - (rkw\_mpf \cdot m \cdot wp1\_14)\} \\
&\quad +kw\_chk \cdot \{-wp1\_14 + (\beta \cdot w)\} && (3.6)\\
w' &= kw\_mpf \cdot \{wp2 - (rkw\_mpf \cdot m \cdot w)\} \\
&\quad -kw\_chk \cdot \{-wp1\_14 + (\beta \cdot w)\} && (3.7)\\
wp1p2' &= -kw\_mpf \cdot \{wp1p2 - (rkw\_mpf \cdot m \cdot wp1\_14)\} \\
&\quad +kw\_chk \cdot \{-wp1p2 + (\beta \cdot wp2)\} && (3.8)\\
myt' &= kmyt \cdot \{-m \cdot myt + \gamma(Tmy - myt)\} && (3.9)
\end{aligned}
$$

- Lamin phosphorylation, Nuclear envelope breakdown (NEB)

$$
\begin{aligned}
lp' &= kla \cdot m \cdot (Tl - lp) && (3.10)\\
fNEB &= (lp - zz)/(Tl - zz) \cdot heav\{(lp - zz)/(Tl - zz)\} && (3.11)
\end{aligned}
$$

The equations for lamin phosphorylation and NEB are introduced to compare the model with the available NEB data. They do not show up in the wiring diagram, and are just a means to relate MPF activity to NEB. These equations are taken directly from Marlovits et al. (1998). It is known that even a small amount of MPF will cause NEB after sufficient time. It is also known that lamin proteins, a part of the nuclear envelope, are phosphorylated by MPF (Nigg, 2001). These equations assume that the NEB starts only after a threshold fraction (zz) of lamins are phosphorylated, and the fraction of NEB (fNEB) is a linear function of the fraction of phosphorylated lamins.

- Auxiliary equations (used in above equations)

$$
\begin{aligned}
c &= Tc - cp285 - cp287 - cp287\_14 && (3.12)\\
wp2 &= Tw - wp1p2 - wp1\_14 - w && (3.13)
\end{aligned}
$$

where $Tc =$ "total Cdc25" and $Tw =$ "total Wee1".

Part A			
Dimensionless		$\min^{-1}$	
rkm	19	km	0.45
$rkc285$	0.0132	kw_mpf	0.27
rkw_mpf	5	$kc285$	6.485
Tc	1	$rkmc$	0.00706
Tw	1	$rkmw$	0.0
Tl	1	kla	0.5
zz	0.7	$k1$	0.0026
Part not-A			
Dimensionless		$\min^{-1}$	
α	0.1	kw_chk	0.1
β	0.05	$kmyt$	30
γ	0.001	$kc287$	0.05
ω	10	$kc287\_14$	0.3
Tmy	1		

Table 3.1: Parameters in the wiring diagram of Fig.[2.4] and Eqn.[3.1–3.13]. Note that $\alpha = \alpha_0 + \alpha_u$ and $\beta = \beta_0 + \beta_u$, where $\alpha_0 = 0.1,\ \beta_0 = 0.05$ and $\alpha_u = \beta_u = 0$ for normal cell cycle. With UR-DNA resulting from 1000 nuclei/μl and 100 μg/ml of aphidicolin, $\alpha_u = 0.65,\ \beta_u = 0.05$.

Variable name	Interphase	Mitosis
Tm	0.05	1.0
m	0.01	0.9401
$cp285$	0.01	0.9618
$cp287$	0.1	0.002226
$cp287\_14$	0.8	0.022396
$wp1\_14$	0.05	0.0083536
w	0.8	0.16707
$wp1p2$	0.1	0.039265
myt	0.95	0.0010626
lp	0.001	0.99999

Table 3.2: Initial conditions of state variables. The mitotic conditions were derived from the interphase conditions after integrating the model equations for a long time with Tm as a parameter and value 1.0. As expected during mitosis, most of MPF (Tm) is in m, Cdc25 is in $cp285$, most Wee1 in $wp1$ ($=Tw - wp1\_14 - wp1p2 - w$), and most Myt1 and lamins are phosphorylated ($myt \approx 0,\ lp \approx 1$).

3.2 Consequences for Cdc25 and Wee1 subsystems

We have hypothesized that during the unreplicated DNA checkpoint, the kinase activities of checkpoint proteins – Chk1 and other kinase(s) – towards their substrates are increased. This we hope to incorporate using the parameters α and β. $\alpha = \alpha_0 + \alpha_u$ and $\beta = \beta_0 + \beta_u$, where $\alpha_0 = 0.1,\ \beta_0 = 0.05$ and $\alpha_u = \beta_u = 0$ for normal cell cycle.With UR-DNA equal to 1000 nuclei/μl and 100 μg/ml of aphidicolin, $\alpha_u = 0.65,\ \beta_u = 0.05$. Does our hypothesis make sense?

For the Cdc25 subsystem, the total Cdc25 is constant:

$$cp285 + c + cp287 + cp287\_14 = Tc \tag{3.14}$$

For each of the reaction involved, at equilibrium:

$$\frac{m \cdot c}{cp285} = rkc285,\ \frac{cp287}{c} = \alpha,\ \frac{cp287\_14}{cp287} = \omega \tag{3.15}$$

Using above relations in the conservation relation (Eqn. 3.14), writing it only in terms of cp285, gives:

$$cp285 \quad = \quad \frac{Tc \cdot m}{m + rkc285(1 + \alpha + \alpha\omega)} \tag{3.16}$$

A plot of equation (3.16) is shown in Fig. [3.1a]. We see that increasing α implies a higher value of MPF needed to activated Cdc25. Thus our hypothesis is confirmed for Cdc25.

A similar calculation for Wee1 using its conservation relation, yields the following relation:

$$wp1\_14 \quad = \quad \frac{Tw}{(1 + \frac{1}{\beta})(1 + rkw\_mpf \cdot m)} \tag{3.17}$$

The plot of equation (3.17) in Fig. [3.1b] shows that increasing β increases the apparent value of Tw and the value of MPF at which Wee1 inactivates, thus enhancing Wee1's effect and delaying the MPF activation and entry into mitosis.

We have thus confirmed that the hypothesis is workable.

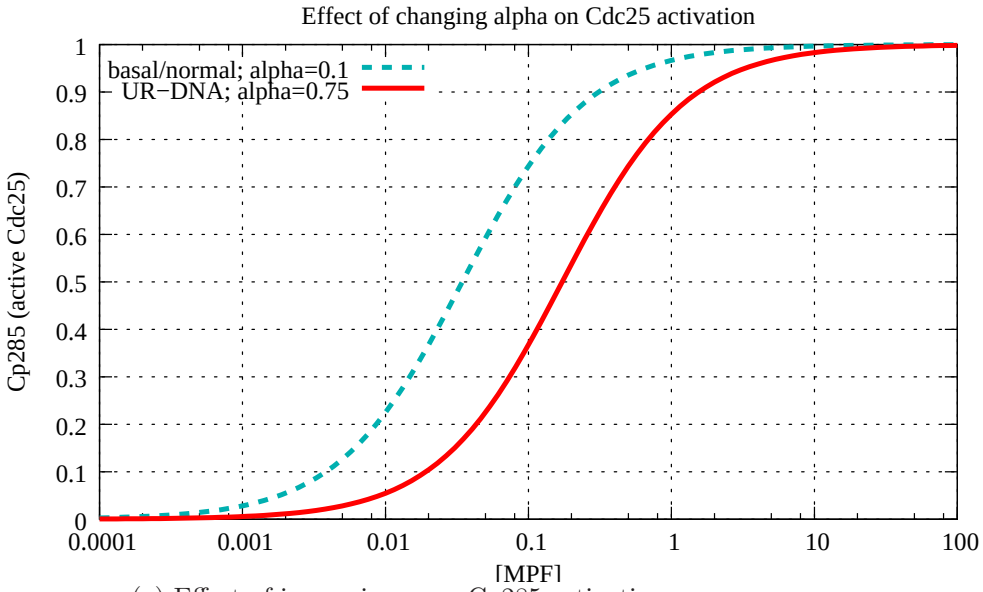

(a) Effect of increasing α on Cp285 activation.

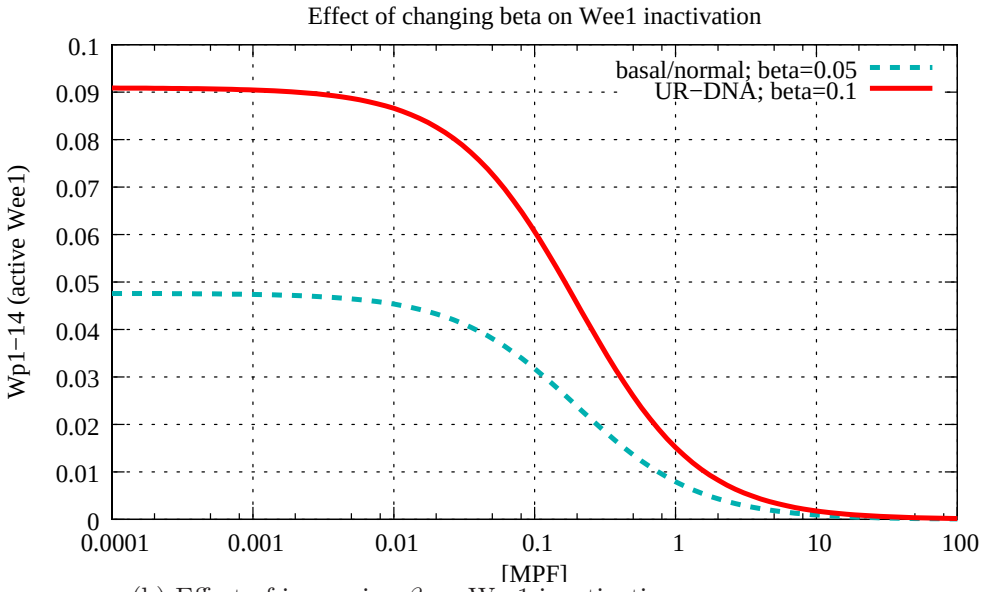

(b) Effect of increasing β on Wee1 inactivation.

Figure 3.1: Change in MPF thresholds for Cdc25 activation and Wee1 inactivation. According to our model, presence of UR-DNA implies an increase in α (and β), thus the above (red) curves imply that more MPF is needed for Cdc25 activation (and Wee1 inactivation) and hence entry into mitosis is delayed. Note the logarithmic scale on MPF (horizontal) axis, and that since MPF is scaled to 1, it is always less than 1.

Chapter 4

Results: comparison with data

4.1 Getting suitable parameters

4.1.1 Types of data available

Many experiments in this area are mainly done to uncover the wiring diagram of molecular interactions underlying cellular behavior. Once some portion of the diagram is established, more detailed experiments can attempt to determine the rates of various reactions. Portion A (core cell cycle engine – see Fig.[1.6] on page 10) of our wiring diagram has such detailed information available, whereas for the rest of the diagram, we still need clarification of the wiring of interactions. (By the not-A portion, we mean the parts of the new wiring diagram (Fig.[2.4]) that were absent in Fig.[1.6]. We sometimes call this the "newer portion" of the wiring diagram, and part-A as the "older portion".)

For portion A, a typical detailed experiment is as follows: the extract is arrested in either interphase or mitosis. This is done by inhibiting protein (including cyclin) synthesis to keep the extract in interphase, or using non-degradable cyclin to hold it in mitosis. In this 'frozen' extract, a small amount of some component (say MPF) is added and monitored for the change of its phosphorylation state with time. For example Figures [4.2 – 4.4] starting from page 33 are based on such experiments. They were used for parameter estimation on the (older) portion A of the model.

At present, two main kinds of information about the new portion are available:

%NEB data To monitor the extract's entry into mitosis, it is supplemented with sperm nuclei. The nuclear envelope breakdown (NEB) of these nuclei is an indicator of MPF activity (like *in vivo*). When a majority of nuclei have broken down, the extract is said to have entered mitosis. This is a practical though not the most accurate indicator of MPF activity. For example, see Fig.[2.3] on page 19.

To compare our model with %NEB data, we added a simple model of lamin protein phosphorylation. These proteins are part of the nuclear envelope and we assume that the phosphorylation of a threshold fraction implies NEB (see equations for lp and fNEB).

Steady state data Here, the 'state' of molecules at interphase or mitosis (with or without any perturbation to the system) is measured. For example, Kumagai et al. (1998b) discovered that during interphase, most Cdc25 is bound to 14-3-3 (see Fig.[4.1]).

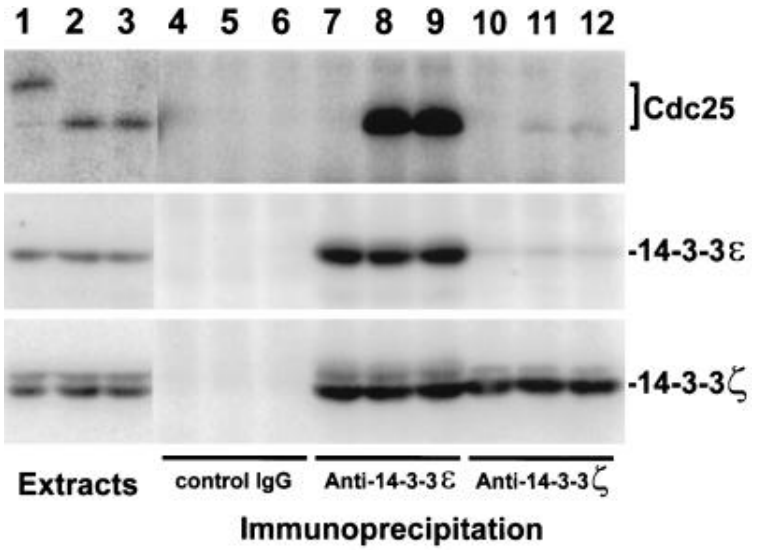

Figure 4.1: Example of steady-state data. Two microliters of M-phase extract (lane 1), interphase extract containing no sperm nuclei (lane 2), and interphase extract containing 3000 UV-damaged sperm nuclei/μl (lane 3) were subjected to SDS-PAGE and immunoblotted with anti-Cdc25 antibodies (top), anti-14-3-3 antibodies (middle), or anti-14-3-3 antibodies (bottom). One hundred microliters of M-phase extract (lanes 4, 7, and 10), interphase extract containing no sperm nuclei (lanes 5, 8, and 11), and interphase extract containing 3000 UV-damaged sperm nuclei/μl (lanes 6, 9, and 12) were immunoprecipitated with control antibodies (lanes 4,6), anti-14-3-3 antibodies (lanes 7,9), or anti-14-3-3 antibodies (lanes 10,12). Immunoprecipitated proteins were separated by SDS-PAGE and immunoblotted with anti-Cdc25 antibodies (top), anti-14-3-3 antibodies (middle), or anti-14-3-3 antibodies (bottom). All extracts contained 100 μg/ml cycloheximide. *Source:* Kumagai et al. (1998b, Fig. 5) - requested for permission.

4.1.2 Parameters of the established (part-A/older) portion of the wiring diagram

In our modeling of the cell cycle, we believe that its bistable nature is a key characteristic. We therefore started with a simple three variable (MPF, Cdc25, Wee1) model of the cell cycle using just mass-action kinetics, got parameters that gave us this bistable character, and optimized this parameter set using a parameter optimizer developed in the Tyson lab (Zwolak et al., 2004a,b).

We started from a wiring diagram with only three elements – MPF, its activating phosphatase Cdc25, and its inactivating kinase Wee1 – using only mass action kinetics. No such purely mass-action based model has been published previously by the Tyson group. We started with a simplified wiring diagram with two forms each of MPF, Cdc25, and Wee1, with the total amount of each molecule being constant (hence 3 variable model). Then, to get a parameter set that would give multiple steady states, we used a program called the Chemical Reaction Network Toolbox

(CRNT) (Feinberg and Ellison, 1999). In response to a user-specified reaction network, the 'Network Analyst' portion of CRNT, will try to determine if there can be rate constants such that the resulting differential equations admit oscillations, an unstable steady state, multiple steady states, a degenerate steady state (i.e., one with a zero eigenvalue), and so on. When the Network Analyst determines that the answer is no, it will tell you so. On the other hand, if Network Analyst determines, for example, that a reaction network has the capacity for multiple steady states, it will exhibit a sample set of rate constants along with a pair of steady states consistent with them.

Using bifurcation analysis, we analyzed the simple model around this parameter set given by CRNT. After the simple modification of including a basal phosphatase activity on MPF in the absence of Cdc25, we were able to get the expected bistable nature. More details about the working of CRNT, and how we used it for model building can be found in Appendix [A] on 43.

To get a model that would account for experimental observations, we input this simple model into a parameter optimizer developed in the Tyson lab (Zwolak et al., 2004b,a). The parameter set given by CRNT (after adding the constant to get bistable nature) was used as the initial guess. First global and then local optimizers of this program were used to get a 'reasonable' parameter set. Appendix [A] on 43 has information about both our use of CRNT and the parameter optimizer. The optimized values appear in Table [3.1]. Table [A.1] on page 51 at the end of that section shows the results of optimization of the mass-action based simple model and the corresponding parameters of the new model.

Then, the wiring diagram was updated to include the new experimental information about checkpoint activation. The parameters estimated by the optimizer were carried over as-is to the more detailed model. See table 3.1 for the parameter values in the established portion (part-A).

4.1.3 Parameters of the non-established (not-A/newer) portion of the wiring diagram

The additional parameters introduced due to expansion of the wiring diagram were estimated 'by hand' based on the two forms of experimental information available. (The nature of this information was detailed at the start of this section). This data on the not-A/newer portion of the wiring diagram is less decisive and more obscure. Here we attempt to fix many of the new parameters based on this data.

The parameters needed to incorporate the not-A into the model may be classified as:

- Dimensionless (Steady-State) Constants: α, ω, β, γ;
- Rate Constants (min^{-1}): $kc287$, $kc287\_14$, kw_chk, $kmyt$.

We see from the equations (Eqn.[3.1-3.13]) that the dimensionless constants decide where the steady-state of each pair of reactions lies, and the rate constants decide the rate at which it is approached. For instance, ω (in Eqn.[3.5]) has a value of 15 implying that at steady-state, $[cp287\_14]$ is 15 times $[cp287]$, and $kc287\_14$ s^{-1} is the rate at which this state is approached. For portion

B, the steady-state experimental data can give an estimate of the dimensionless constants and in some places, comparisons with the portion A of the model can give estimates of the rate constants. This way we hope to justify the complete model - the wiring diagram, the rate laws, and the parameters. Below, we attempt to defend the basis of the parameter choices for the not-A portion of the wiring diagram. Our main tool for parameter twiddling was the range-integration option in XPPAUT (Ermentrout, 2002), where one can step through values of one or two parameters over chosen range(s) and see how this changes the results.

ω : $\omega = 10$ implies that 10·[Cp287] = [Cp287_14] at steady state. Most ($> 85\%$) of Cdc25 seems to be bound to 14-3-3 (Kumagai et al., 1998b, pg. 350) during interphase.

β : basal value of $\beta = 0.05$ implies that [Wp1_14] = 0.05·[W], and [Wp1p2] = 0.05·[Wp2] at steady state. (In the presence of aphidicolin $\beta = 0.1$.). This value was chosen based on (Lee et al., 2001, Fig.1) which indicates that about 5% of Wee1 is bound to 14-3-3 during interphase. When Chk1 is depleted we set $\beta = 0.01$. (It is known that depletion of Chk1 causes an advance in the NEB of the normal cell cycle (Kumagai et al., 1998a).)

α : Since at steady-state, α·[Cp287] = [C], a basal value of $\alpha = 0.1$ implies that [C] = 0.1· [Cp287]. (In the presence of aphidicolin $\alpha = 0.75$.) We do not know of any experiment that indicates the amounts of Cdc25 in these two forms during interphase, hence we started by assuming that $\omega = 10$, $\beta = 0.05$, and then fiddled with the values of parameters $k1$ and α that gave decent fits to the %NEB data. This value was chosen in the following way: we fixed the parameters of the portion A of the wiring diagram using the parameter estimator (on a simpler 3 variable model). Then we carried over these parameters to the larger wiring diagram (with both part A and not-A included). We then attempted to fit the older experiments (used by the parameter estimator) and the newer data (%NEB data including Chk1, etc.).

γ : $\gamma = 0.001$. myt = "total myt"/2 = $Tmy/2$ when $m = \gamma$ (since at steady-state, $myt = Tmy/(m/\gamma + 1)$) – a very small value compared to the activation threshold (of $m \approx 0.06$). We don't know of any experiments to fix this value. Our main reference was Mueller et al. (1995b).

$kmyt$: $kmyt = 30$. This value was chosen to be of a reasonable magnitude while allowing γ to be large.

$kc287$: $kc287 = 0.05$. Using XPPAUT (range integration), we analyzed the behavior of the normal cell cycle while changing this parameter over the range of 0.001 to 10. fNEB, our variable corresponding to %NEB, was very sensitive to $kc287$ from $0.001 \rightarrow 0.01$, and became less sensitive after that. Further, in the experiment shown in Fig.[4.3,(b)], the ratio of $kc287/kc285$ decides the amount of active labeled Cdc25 seen. A value of $kc287$ larger than 1 would make the simulation of this experiment incompatible with data. These two considerations led to the choice of $kc287 = 0.05$.

$kc287\_14$: $kc287\_14 = 0.3$. We analyzed the behavior of the normal cell cycle while changing this parameter over the range of 0.001 to 10. The NEB was not very sensitive to the value of $kc287\_14$. However, for values for values > 0.1, $cp287\_14$ and NEB timing hardly changed. Also, from Margolis et al. (2003, Fig. 5A), it takes about 10 minutes for Cdc25:14-3-3 binding

to be lost. This implies a half-life of about 2-3 minutes. Therefore, based on Eqn.[3.5], we chose $kc287\_14$ as 0.3 ($\approx \ln(2)/2.5$).

kw_chk : $kw\_chk = 0.1$. NEB of the normal cell cycle was sensitive to this parameter from $0.001 \rightarrow\sim 0.05$, becoming very less sensitive for the larger value (0.05). Hence, we chose $kw\_chk = 0.1$.

4.2 Simulations of experiments

4.2.1 Older experiments

In Figures 4.2 (pg. 33), 4.3 (pg. 34), and 4.4 (pg. 35), we show the plots of experimental data and corresponding simulations of the model. These experiments were fit using the parameter optimizer (Zwolak et al., 2004b,a) on the simple three variable model (Eqn. [A.6, A.8]).

4.2.2 New nuclear envelope breakdown (NEB) type data

Many experiments since 1998 have attempted to untangle the UR-DNA checkpoint pathway. These experiments, though not very quantitative, are general indicators of how the checkpoint works. The experiment shown in Figure [4.6], where the depletion of Wee1 did not affect the NEB significantly, is a case in point. Considered with the inconclusive evidence about how Wee1 takes part in the UR-DNA checkpoint (Lee et al., 2001, discussion section), this data led us to reconsider our wiring diagram. (See the model-making process depicted in Fig.[1.7]) For our simulation to match experiments, we needed to include another kinase. Though there is no direct evidence regarding Myt1 participation in Lee et al. (2001), it suited our purpose (Mueller et al., 1995b) as the most significant kinase of MPF (that is unaffected by the checkpoint). However Lee et al. (2001, discussion section) suggest one other possible hypothesis that may explain this situation. They suggest that a small fraction of Wee1 that gets incorporated into nuclei may be responsible for the checkpoint response through Chk1, and that there are technical limitations to assay this Wee1. This they hypothesize based on following facts: Immunoprecipitation of Chk1 does not affect binding of 14-3-3 to Wee1; binding to 14-3-3 does not seem to increase the kinase activity of Wee1 (immunoprecipitated from aphidicolin treated extracts); only 5% of Wee1 appears to be bound to 14-3-3; Wee1 is differentially localized in the nucleus depending on binding to 14-3-3; approximately 10% or less of Wee1 in extracts gets incorporated into nuclei in extracts. For modeling this, we may need to introduce compartments in our model (or more forms of Wee1). (Here it is taken care of by a small value of β.) However, the compartments are created in extracts only when the sperm nuclei are added for monitoring cell cycle phases. With the goal of better representing the *in vivo* cell cycle in frog eggs and embryos, it seems that compartmentalization may be unavoidable in future models.

The Cdc25 related experiments are depicted in Fig.[4.7]. A mutant form of Cdc25 that cannot be phosphorylated on S-287 was added to frog egg extracts in the absence or presence of unreplicated DNA. Recall that the phosphorylation on S-287 is necessary for the binding of Cdc25 to 14-3-3 and that it is mutually antagonistic with the activating phosphorylation on S-285 (see Chapter [2] and the wiring diagram in Fig.[2.4]). For simulating the Cdc25 that was added to aphidicolin treated

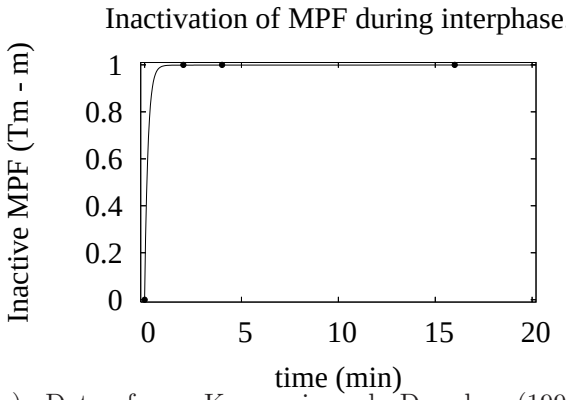

(a) Data from Kumagai and Dunphy (1995, Fig. 3C). Allowed estimation of parameter(s): rkm, km.

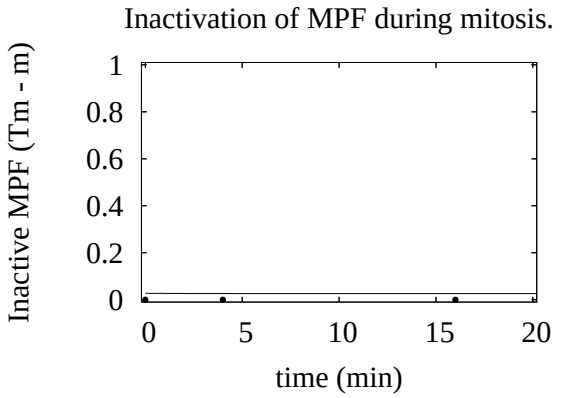

(b) Data from Kumagai and Dunphy (1995, Fig. 3C). Allowed estimation of parameter: $rkmw$.

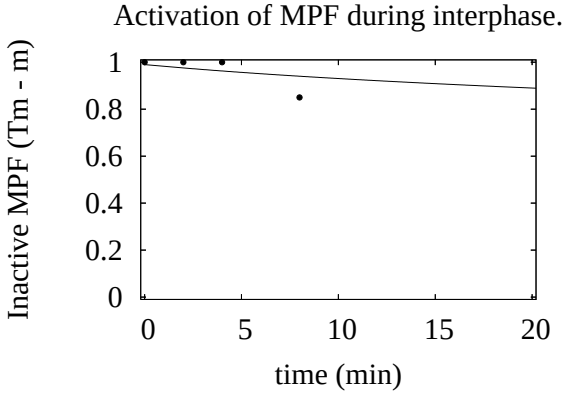

(c) Data from Kumagai and Dunphy (1995, Fig. 4B). Allowed estimation of parameters: km, $rkmc$.

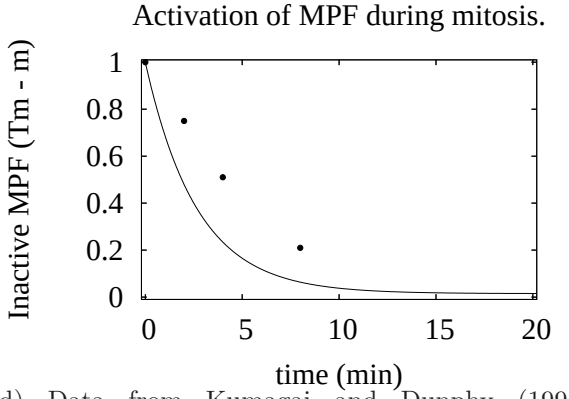

(d) Data from Kumagai and Dunphy (1995, Fig. 4B). Allowed estimation of parameters: km, $rkmc$.

Figure 4.2: MPF activation and inactivation during interphase and mitosis. Solid line indicates model simulation and dots are the experimental data. In the experiment for (a) and (b), active MPF with a radiolabelled phosphate group on T-161 was added to interphase or mitotic extracts. For (c) and (d), a complex between cyclin-B and recombinant Cdc2 that was radiolabelled with ^{32}P on Y-15 was added to extracts in I and M phases.
For simulating the experiments, the model was supplemented with an additional equation for labeled MPF: (a), (b), and (d) had an equation that was exactly same as equation [3.2] with parameter $Tlm = Tm = 1.0, k1 = 0$; (c) had only the phosphatase half of the equation [3.2], i.e., $\dot{lm} = km{\cdot}(cp285{+}rkmc){\cdot}(Tlm{-}lm)$. In all cases, we consider the effect of additional components on the cell cycle machinery as insignificant. Mitotic simulations used the initial conditions shown in Table [3.2] on pg. 25.

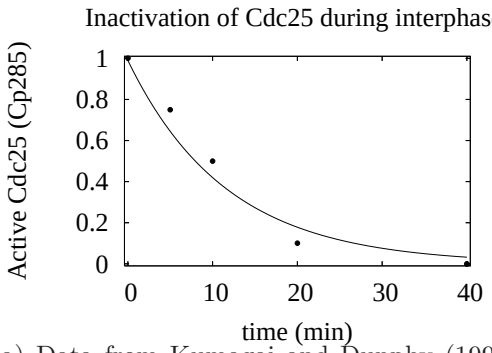

(a) Data from Kumagai and Dunphy (1992, Fig. 10B). Allowed estimation of parameter(s): $kc285$, $rkc285$. [1]

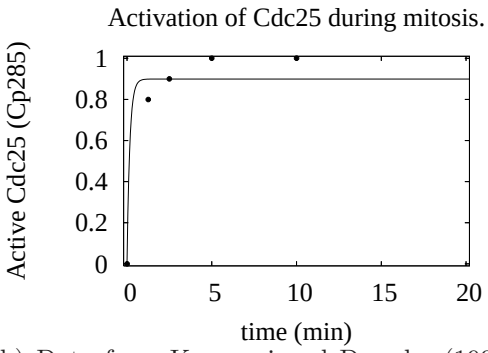

(b) Data from Kumagai and Dunphy (1992, Fig. 10A). Allowed estimation of parameter: $kc285$.

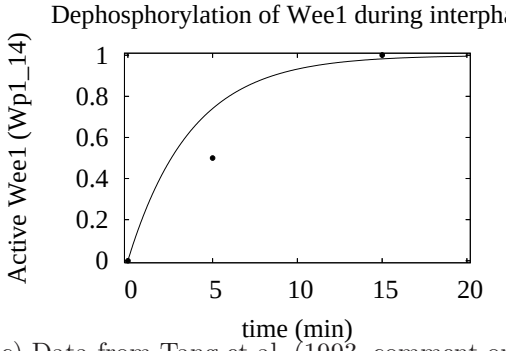

(c) Data from Tang et al. (1993, comment on pg. 3430). Allowed estimation of parameters: kw_mpf, rkw_mpf.

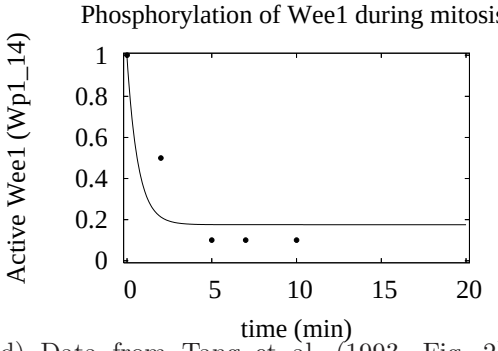

(d) Data from Tang et al. (1993, Fig. 2). Allowed estimation of parameters: kw_mpf, rkw_mpf.

Figure 4.3: Cdc25 and Wee1 activation and inactivation in I and M phases. Solid line: model simulation, dots: experimental data. For (a), *Drosophila* Cdc25 was incubated in I phase extract; For (b), ^{35}S labeled recombinant Cdc25 was added to CSF extract. For (d), Wee1 protein from Sf9 cell lysate was added to CSF-arrested extract (simulates mitotic extract); For (c), the addition of $CaCl_2$ to the extract in (d) resulted in a restoration of the Wee1 protein to its original form within 15 minutes (the data point at 5 minutes was made-up assuming 15 minutes = 3 half-lives).
For simulating the experiments, the model was supplemented with additional equation(s). *For (a) and (b)*, the following equations were added:
$\dot{lcp285} = kc285 \cdot (m \cdot lc - (1 - oka) \cdot rkc285 \cdot lcp285)$
$\dot{lcp287} = kc287 \cdot (-(1 - oka) \cdot lcp287 + \alpha \cdot lc)$
with parameter $oka = 0, 1$ for (a),(b) respectively. $oka = 1(0)$ stands for presence(absence) of okadaic acid which blocks dephosphorylation of Cdc25. Additionally $k1 = 0$ and the total labeled Cdc25, $Tlc = (lcp285 + lc + lcp287) = 1$. Supplementary initial conditions, for (a): $lcp285 = 0.99$, $lcp287 = 0.01$, for (b): $lcp285 = lcp287 = 0.01$. We ignore the $Cp287\_14$ form of Cdc25 because it is known that okadaic acid removes 14-3-3 without affecting Ser-287 phosphorylation of Cdc25 (Margolis et al., 2003, Fig.5D,E).
For (c) and (d), one equation for the most potent form of Wee1 was added:
$\dot{lwp1\_14} = kw\_mpf \cdot (lwp1p2 - rkw\_mpf \cdot m \cdot lwp1\_14)$
with $Tlw = lwp1\_14 + lwp1p2 = 1$. Initial conditions for (c),(d): $lwp1\_14 = 0, 1$ respectively.
In all cases, we consider the effect of additional components on the cell cycle machinery as insignificant. Mitotic simulations in all cases used the initial conditions shown in table [3.2] on pg. 25.

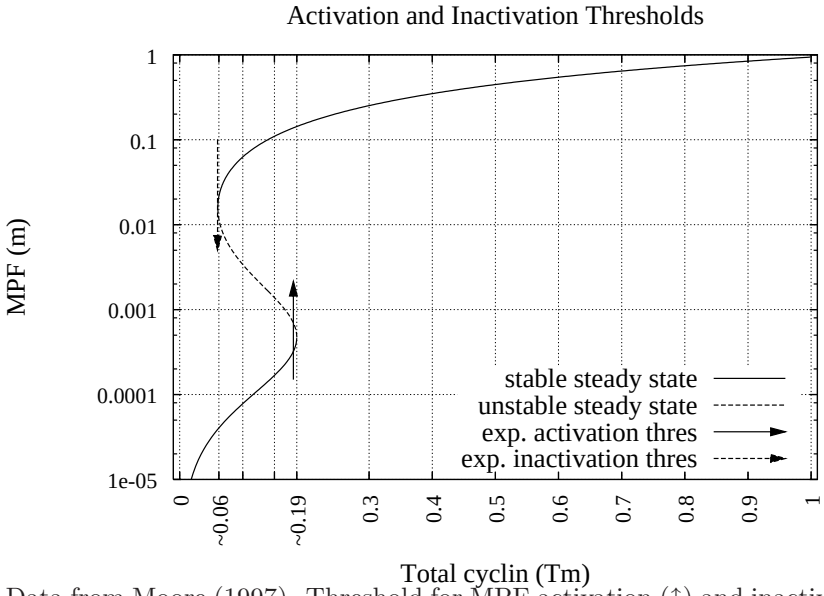

(a) Data from Moore (1997). Threshold for MPF activation (↑) and inactivation (↓). Mainly allowed the estimation of steady-state parameter(s): $rkc285$, rkm (using parameter estimator); α, β, γ (very sensitive).

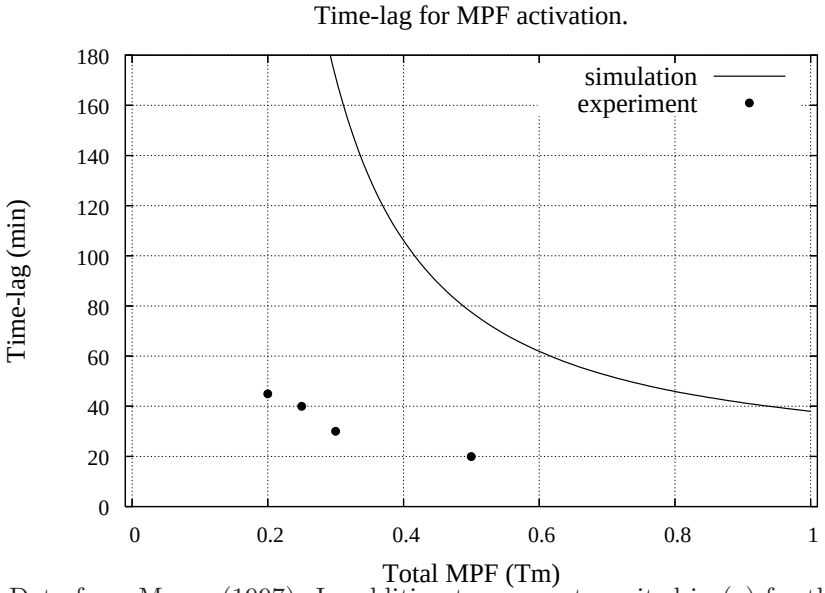

(b) Data from Moore (1997). In addition to parameters cited in (a) for threshold data, this allowed estimation of the rate-constant parameters: km, $kc285$, kw_mpf. This fit may be improved by using parameter estimation on the complete model.

Figure 4.4: Threshold and time-lag data. In (a), the hysteresis plot was created using `XPPAUT` (Ermentrout, 2002). In (b), the simulation plot was created from closely spaced data points that were used to interpolate a cubic spline (using `gnuplot`). For both (a) and (b), the equation for Tm was removed and it was made a parameter; the rest of the parameters remained the same as the original model.

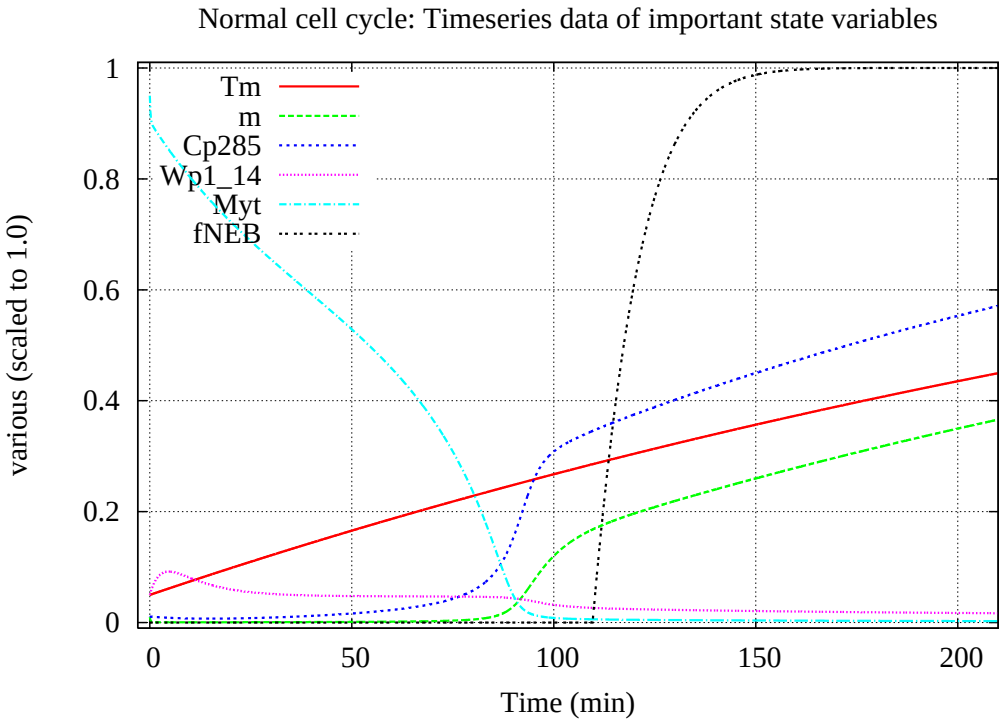

Figure 4.5: Time series of a normal Cell Cycle.

extracts, we supplemented the normal model with some equations. This and parametric details are given in the description of the Figure (4.7).

Simulations of the Wee1 experiments (Fig.[4.6]) were carried out by setting parameters aw, α, and β. For simulating Wee1 depletion, we set $aw = 0$ in Eqn.[3.2], thus cutting-off the feedback of Wee1 on MPF. Presence of UR-DNA in the presence of DNA replication inhibitor aphidicolin (+Aph) was simulated by increasing $\alpha : 0.1 \rightarrow 0.75$, $\beta : 0.05 \rightarrow 0.1$, thus increasing the kinase activity of Chk1, or another kinase acting on the same substrates. Chk1 depletion in presence of UR-DNA (-Chk+Aph) was simulated using $\alpha : 0.1 \rightarrow 0.45$, $\beta : 0.05 \rightarrow 0.01$. Data from Lee et al. (2001, Fig. 5C) was used for this, and is shown with data from Lee et al. (2001, Fig. 5B) because the +Aph and -Wee+Aph parts of both figures are identical (though normal cell cycles differ by about 15 minutes). Note that the reduction in β below basal value effectively cuts down the effect of Wee1 in absence of Chk1, while α is between basal and +Aph values.

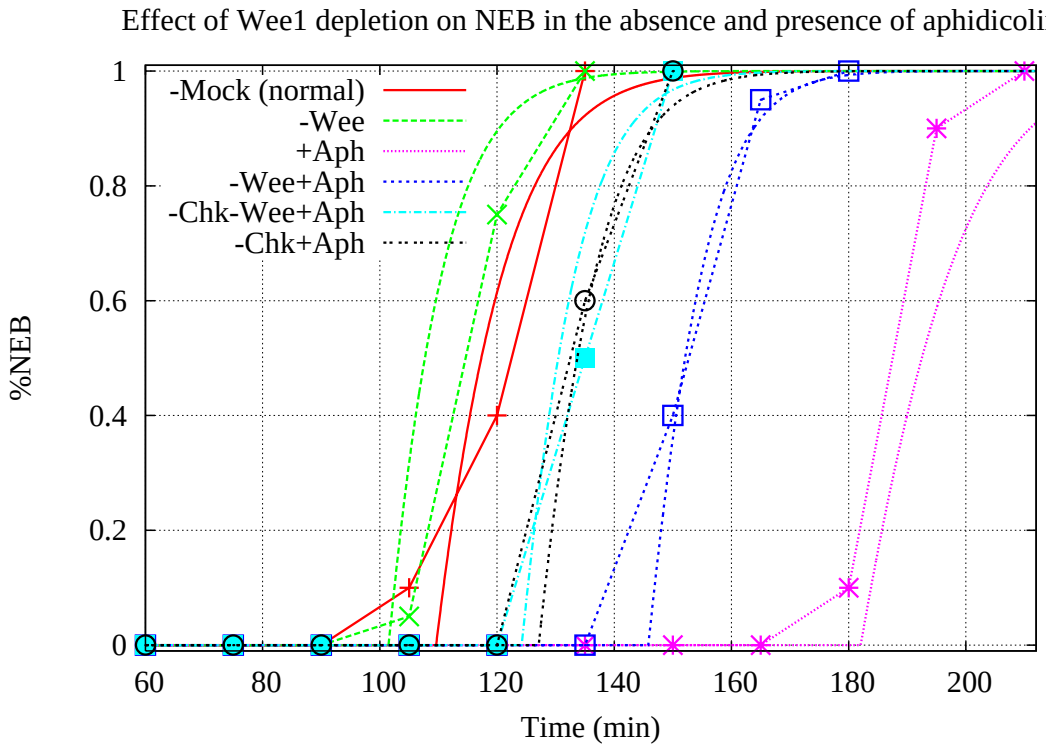

Figure 4.6: Effect of Wee1 depletion on %NEB in presence/absence of aphidicolin and Chk1. Smooth curves are model simulations. Experimental data from Lee et al. (2001, Fig. 5B,C). Used for setting parameters α and β. Following settings were used for each simulation:
-Mock: $k1 = 0.0026$ (applied for all), -Wee: $aw = 0$, +Aph: $\alpha = 0.75$, $\beta = 0.1$ (normally, $\alpha = 0.1$, $\beta = 0.05$), +Aph-Wee: $\alpha = 0.75$, $\beta = 0.1$ and $aw = 0$, -Chk+Aph: $\alpha = 0.45$, $\beta = 0.01$. The data for the -Chk experiments was taken from (Lee et al., 2001, Fig. 5C).

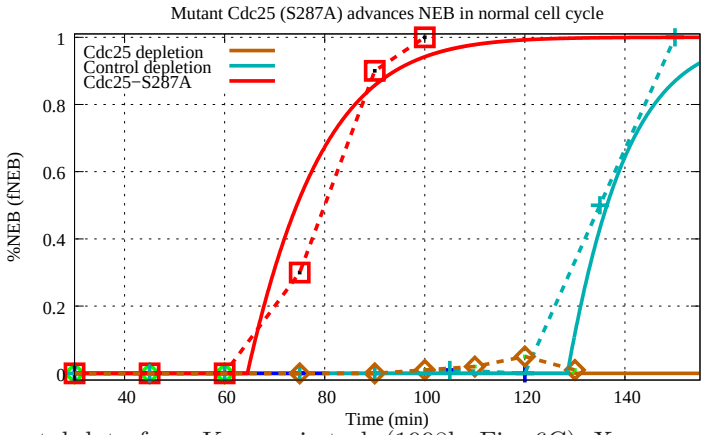

(a) Experimental data from Kumagai et al. (1998b, Fig. 6C). Xenopus egg extracts were immunodepleted with anti-Cdc25 antibodies. To the Cdc25 depleted extracts, His6-Cdc25, or His6-Cdc25-S287A were added to a final concentration equal to the original concentration of Cdc25.

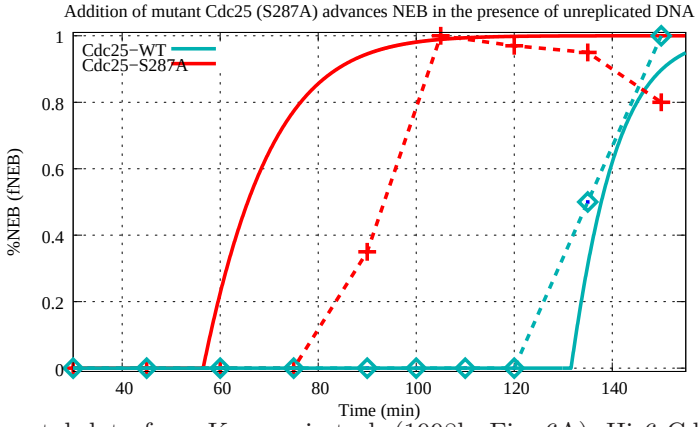

(b) Experimental data from Kumagai et al. (1998b, Fig. 6A). His6-Cdc25 or His6-Cdc25-S287A were added to the interphase egg extracts containing aphidicolin. Unlike (a), endogenous Cdc25 was not depleted in (b).

Figure 4.7: %NEB experiments with mutant and wild-type Cdc25 without or with unreplicated DNA (due to the presence of aphidicolin). Smooth curves are simulations. Experiments were done as explained below each figure. Aliquots were taken at indicated times and NEB was monitored by microscopy. *For simulating (b)*, the model was augmented with following equations: $\dot{cap}285 = kc285(m \cdot cn285 - rkc285 \cdot cap285)$, $\dot{cap}287 = kc287(-cap287 + a \cdot \alpha \cdot cn285)$, $\dot{cap}287\_14 = a \cdot kc287\_14 \cdot (-cp287\_14 + \omega \cdot cp287)$, where $cn285 = Tca - cap285 - cap287 - cap287\_14$. Parameter values were $Tca = 1$, $\alpha = 0.75$, $\beta = 0.1$ (without UR-DNA, $\alpha = 0.1$, $\beta = 0.05$). For S287A we set $a = 0$, with initial conditions (ICs): $cap285 = 0.1$, $cap287 = 0.0$, $cap287\_14 = 0.0$; For WT, $a = 1$ with initial conditions of additional Cdc25 same as in the original model (refer Tab.[3.2] on pg. 25). *For simulating (a)* with S287A, we set ICs as for additional Cdc25 in (b) (see above); for WT, normal ICs were used (refer Tab.[3.2]). No additional equations were needed for (a). In (a), we considered the control depletion in (Lee et al., 2001, Fig.6C) to be closer to the normal cell cycle (instead of Cdc25-WT) for comparison with simulations. We could have done the same by using the 'buffer' data for normal cell cycle in (b), but the data was collected only until 150 min and does not indicate when entry into mitosis occurred. To match both WT and S287A curves, we would also need to reduce the rate of cyclin synthesis by 25% for this purpose.

Chapter 5

Discussion and future work

5.1 Discussion

We have created a model of the unreplicated DNA (UR-DNA) checkpoint induced in the extracts of *Xenopus* eggs. This extract system is an *in vitro* model of the *in vivo* cell cycle of these extracts.

Our approach to modeling is a step by step process. We believe this to be a reasonable approach in the face of incomplete information about such a complex system. Inadequate means to understand and analyze large complex systems is also a significant reason. For instance, given all the known elements in the extracts of frog eggs, and incomplete information about their interactions, we do not know any algorithm/method to get bistable MPF dynamics (as observed by experiments) for the complete system. However, we are able to get bistable behavior in a reduced three variable system (that we can understand) and then attempt to retain it as we enlarge the system by including more components. Therefore, to reduce the complexity, we have not considered the effects of all known components. This type of modeling may be termed phenomenological.

Our model-making started from a simple three variable model based on mass-action kinetics (Eqn. [A.6,A.8]). This model assumes a single kinase acting against MPF and a single phosphatase, Cdc25, supporting activation of MPF. We found out using the program CRNT and using bifurcation analysis that we could get bistable dynamics from this system (Fig.[A.2]). Parameter estimation on this smaller system was used. These parameters were used in a larger, more detailed model that includes parameters for incorporating UR-DNA effects (see table [A.1]). The comparison of the final model with some experiments appears in Fig. [4.2 – 4.6].

The immediate ancestor of the model (Eqn.[3.1 – 3.13]) considered only the 14-3-3 bound Wee1 – the most potent form of Wee1 (Lee et al., 2001) – to be the kinase affecting MPF. To incorporate the experiment where Wee1 depletion doesn't affect the timing of NEB (Fig.4.6), we had to add another kinase, Myt1, and make it more significant ($am = 0.7,\ aw = 0.3$ in Eqn.[3.2]). Because Myt1 is known to be a membrane associated protein, and a membrane does form around demembranated sperm DNA that are added to extracts for monitoring cell cycle phases, we assume Myt1 is present. The reason why Wee1 depletion does not affect the NEB timing is then presumably a consequence

of the presence of Myt1. Experiments that determine this would clarify the picture. Myt1 (and its activity as an MPF kinase) appears unaffected by the UR-DNA checkpoint (Mueller et al., 1995b, Fig. 5). We have, however, ignored the activity (apparently 1/5 of active Myt1) of the phosphorylated Myt1 that accumulates during progress into mitosis.

Our model considers only the 14-3-3 bound form of Wee1 to be the active form. This form is about 5% of total Wee1 (Lee et al., 2001, Fig. 1C). *In vitro* experiments show that the activity of 14-3-3 bound form is about twice that of the other three forms (Lee et al., 2001, Fig. 4E). However, it is also known that the 14-3-3 form is evenly distributed in the nucleus; the unbound form existing in punctate structures (Lee et al., 2001, Fig. 3). This may lead to a much higher activity of the 14-3-3 form than indicated by the *in vitro* experiments. The 14-3-3 form being 5% was translated into the basal value of $\beta = 0.05$. That only this form that is present in a small amount is considered active allows the NEB timing to remain unaffected by Wee1 depletion. Another reason for making this simplifying assumption was our inability to get appropriate parameters (by hand) when both $wp1\_14$ and w are considered active (with w considered 1/5 as active as $wp1\_14$). Lee et al. (2001) presents the only available data on checkpoint activation of Wee1 through Chk1 and 14-3-3. Thus, in general, there is a need to clarify what kinase acts on MPF and how it is regulated during the checkpoint.

Our simulations of perturbation in the Cdc25 portion of the system do not completely agree with the experiments (Fig. 4.7). Part (a) of this figure compares well with experiments. Part (b) of this figure has a difference of about 20 minutes for 0.5 NEB with Cdc25-S287A. In NEB experiments, a variation of about 10-15 minutes is considered common, and we have used a lower value of $k1 = 0.0021$ (instead of 0.0026) to match the control (or Cdc25-WT) simulations to experiments. In both (a) and (b), simulations for Cdc25-S287A indicate that the addition of S287A form of Cdc25 'short-circuits' the normal cell cycle progress. A closer look at both (a) and (b) shows that the timing of NEB for the experiment with S287A form in (b) is faster than in (a) due to the presence of both Cdc25-WT and Cdc25-S287A. The major disagreement between simulations and experiment for the S287A form in (b) may be either due to inappropriate parameter values or due to some missing part of the model.

The one parameter bifurcation diagram in Figure [5.1] represents the core of our story. It reflects our belief that the system (and hence our model) is bistable, and that the effect of UR-DNA is to change this basal picture by increasing the thresholds for activation and inactivation. This is how the cell cycle in frog-egg extracts delays entry into mitosis in the presence of UR-DNA. (This core is identical to the earlier proposition of Novak and Tyson (1993)).

5.2 Future work and the need for collaboration

In a non-linear system such as ours, it is difficult to justify a model as (in)sufficient until a comprehensive search of parameter-space has proved unsuccessful for getting a 'decent' comparison between simulations and the major experiments. The experimental evidence should expose various parts of the system in sufficient detail. Then, inconsistent results compared with simulations during parame-

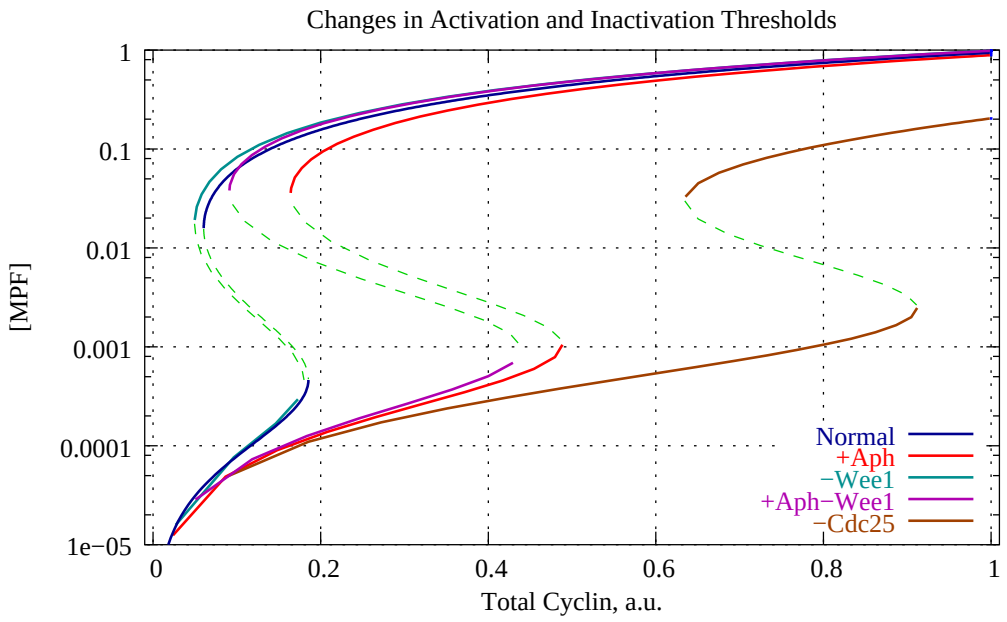

Figure 5.1: Effects of unreplicated DNA and other perturbations on a bistable cell cycle engine. This one parameter bifurcation diagram was generated using `XPPAUT` from Eqn. [3.1 – 3.13]. The equation for Tm was removed and it was treated as the bifurcation parameter. The simulation for '-Cdc25' was done with $Tc = 0.05$, i.e., with incomplete depletion. This is a hypothetical experiment and a potential test of the model.

ter estimation may be interpreted as some flaw in the model. This flaw may be an incorrect rate-law, and/or some missing parts, and/or the break-down of some simplifying assumptions or principles. For instance, having some data on how the various forms of Cdc25 ($cp285$, $cp287$, $cp287\_14$) fluctuate with time during interphase and mitosis in presence and absence of UR-DNA would be very helpful for comparison with simulations. Thus, having sufficiently detailed experimental evidence on various parts of the system and the capability for both global and local parameter searching are crucial to model justification.

Most of the data that we used in our modeling was not intended to be used for that purpose. However, experimental biologists do use this data to theorize about how the system works. We feel that it is inappropriate to use hand-waving arguments about such a non-linear and complex system, where, for instance, there may be signals that cancel each other and only a knowledge of their strengths and temporal variation will let us know what happens. Another example is the prediction and experimental verification (Sha et al., 2003; Pomerening et al., 2003) of the bistable nature of cell cycle in frog extracts. The existence of the two saddle-node bifurcations is closely dependent on the wiring of the model, the rate-laws, and the parameter values used for the model. It seems inappropriate to claim bistability, or justify it, based only on hand-waving arguments. For a better understanding of these complex systems, the kind of modeling done here appears the next logical step after hand-waving arguments. Galileo's principles of motion when translated into Newton's laws of motion increased our detailed understanding of moving systems. The hope

here is to try something similar for biological systems, especially because of their non-linearity and complexity which makes them appear difficult to understand by simpler means.

For proposing and justifying computational models, we need a closer collaboration between the experimental and theoretical parts of the work force. Until now, the drive behind experiments has been creation of wiring diagrams without numbers on them. Mounting evidence about the complexity of biological systems points towards the need for sophisticated approaches for understanding them (Regenmortel, 2004). This requires more elaborate theoretical schemes than wiring diagrams alone. For justification of such models (as here), there is a need for experiments driven by and suitable for comparing with such models (as in Sha et al. (2003); Pomerening et al. (2003)). This collaboration may lead to better experimental and theoretical approaches, and/or enhanced understanding of our limitations in explaining life with present day physical science. In either case, we should understand life better.

Appendix A

Once the wiring diagram has been set up, we need to choose the rate laws and the associated parameters for creating the model. This needs to be done so that the model output is comparable to experimental results. Suppose that based on experimental information we are able to fix the rate laws. Below we describe the tools we used to guide us regarding the parameter values.

A.1 CRNT: Chemical Reaction Network Toolbox

The differential equations of a chemical reaction network and the network structure are closely related. Chemical reaction network theory (Feinberg, 1987, 1988) relates the dynamics of complex isothermal reactors to the structure of the reaction network. If the kinetics are assumed to be mass-action, one is (generally) able to make definite statements like "this system cannot have multiple steady-states", or that "this network can have multiple steady-states and following is an example set of steady-states with rate constants"!

CRNT is a freely available computer program that implements some of the results of chemical reaction network theory (Feinberg and Ellison, 1999). It has two parts, Chemlab and Network Analyst. Chemlab is a simulation environment where one can do experiments with a reaction system (with specific rate constants) by providing initial conditions; it does not concern us here. Network Analyst addresses questions of the following kind: For the given reaction network, are there some (positive) rate constants for which the corresponding differential equations have qualitative property X? where X may be existence of multiple steady-states or periodic oscillations. It is based mostly on deficiency-oriented results of reaction network theory (Feinberg, 1987; Feinberg and Ellison, 1999). For the aid of newcomers, we provide some background information on deficiency theory. This is done by means of the example network that was analyzed for our model. (For detailed explanations, proofs, and further references, please refer Feinberg (1987, 1988, 1995b,a). Many readers may find the manual accompanying the CRNT program sufficient for their purpose.)

Our model network and some terminology

We started model building with the goal to check if bistable nature of the cell cycle could be reproduced by a mass-action based model. We hoped to avoid using Michaelis-Menten enzyme kinetics; see section 1.4 for details of our concerns. For this, we used a simple 3 variable model of the cell cycle with MPF, Cdc25, and Wee1 as the three variables (see Figure [1.6]). With CRNT we hoped to check if this network even allowed multiple steady states. After this, bifurcation analysis could be used to see if we had the bistable nature. Below is the set of reactions for this model that was input into CRNT (Note that *ppab* and *pp*3 are dummy elements that can be eliminated):

$$\begin{aligned} m + c &\longrightarrow m + cp \\ mp + cp &\longrightarrow m + cp \\ cp + ppab &\longrightarrow c + ppab \\ m + w &\longrightarrow mp + w \\ m + w &\longrightarrow m + wp \\ wp + pp3 &\longrightarrow pp3 + w \end{aligned} \tag{A.1}$$

The CRNT program requires one to input the reaction network in terms of the species, complexes, and individual reactions. A *species* is an individual type of molecule taking part in the reactions. Here, we have 8 species: $m, mp, c, cp, w, wp, ppab$, and $pp3$. Thus at any moment, the composition of the reactor can be specified by an N-tuple in $\mathbb{R}^N$. By *complexes* is meant the objects that appear before and after reaction arrows. Our network has $n = 10$ complexes: $m+c$, $m+cp$, $mp+cp$, $m+w$, $mp+w$, $m+wp$, $wp+pp3$, $pp3+w$, $cp+ppab$, $ppab+c$. If we represent each of the species as unit vectors ($\{\mathbf{e}_i\}, i = 1..N$) of $\mathbb{R}^N$, the complexes are sum of these vectors. Let us introduce a numbered labeling scheme to explain: $m = A_1, mp = A_2, c = A_3, cp = A_4, w = A_5, wp = A_6, ppab = A_7, pp3 = A_8$. Let $A_1 = \mathbf{e}_1$, and $A_2 = \mathbf{e}_2$, etc. Then, $m + c = A_1 + A_2 = \mathbf{e}_1 + \mathbf{e}_2$, as so on. If we name the complexes by $\{\mathbf{y}_i\}, i = 1..n$, then each reaction can be denoted as $\mathbf{y}_i \to \mathbf{y}_j$. For this reaction, the *reaction vector* is $\mathbf{y}_j - \mathbf{y}_i$. A reaction network is said to have *rank* s if there exists a linearly independent set of s reaction vectors for the network and there exists no linearly independent set of $s+1$ reaction vectors. For our network, its easy to see that the rank is 3 because all reaction vectors can be written as a linear combination of the 'vectors' $\{m \to mp, c \to cp, w \to wp\}$. Thus, in the vector space ($\mathbb{R}^N$) of species, each complex can be thought of as a point, and each reaction as a vector joining these points; the rank of the network is the maximum number of linearly independent reaction vectors in this space.

$$\begin{aligned} m + c \longrightarrow m + cp \longleftarrow mp + cp \\ mp + w \longleftarrow m + w \longrightarrow m + wp \\ cp + ppab \longrightarrow c + ppab \\ wp + pp3 \longrightarrow w + pp3 \end{aligned} \tag{A.2}$$

Equations [A.2] depict a *standard reaction diagram* of our model network. Each complex appears

only once with arrows indicating the "reacts to" relation between the complexes. A *linkage class* is a set of complexes in a separate "piece" of network. For instance, $\{m + c, m + cp, mp + cp\}$ is a linkage class, as is $\{wp + pp3, w + pp3\}$. From Eqn. [A.2] it is clear that for our model, the number of linkage classes, $l = 4$. *It should also be clear that for any two given networks with the same complexes and linkage classes, the rank of both the networks is the same, i.e., the reaction arrows determine the rank of a reaction network only to the extent that they decide the linkage classes.* Now, for any network with n complexes and l linkage classes, a simple network of $n - l$ reactions can be constructed to give the same linkage classes. (For each linkage class with n_i complexes (where $i \in l$), we need $n_i - 1$ reactions; thus we need $\sum^{l}(n_i - 1) = n - l$ reactions for the complete network.) Hence, for any reaction network with n complexes, l linkage classes, and rank s, we can state that

$$n - l \quad \geq \quad s. \tag{A.3}$$

The **deficiency** of a reaction network is defined as the integer index δ given by

$$\delta \quad = \quad n - l - s. \tag{A.4}$$

From Eqn. [A.3] we see that the deficiency of any reaction network is always non-negative.

We now see how the differential equations based on a reaction network can be written in vectorial terms. Let the instantaneous composition of the reactor be specified by $\mathbf{c} = [c_1, c_2, \ldots, c_N] \in \mathbb{R}^N$. By $\bar{\mathbb{P}}^N$, we mean the non-negative orthant of $\mathbb{R}^N$. Then, for a mass action based system, we have

$$\dot{\mathbf{c}} \quad = \quad \sum_{\mathcal{R}} k_{i\to j} \left(\prod_{L=1}^{N} c_L^{y_{iL}} \right) (\mathbf{y}_j - \mathbf{y}_i), \tag{A.5}$$

where $\mathcal{R}$ is the set of all reactions in the network and y_{iL} is the stoichiometric coefficient of of the species A_L in the reactant complex $\mathbf{y}_i$. Equation [A.5] shows that for any composition $\mathbf{c}$, the corresponding value of $\dot{\mathbf{c}}$ is always a linear combination of reaction vectors. The *stoichiometric subspace* of a reaction network is the set of all linear combinations of the reaction vectors of the network. It should be clear that the dimension of the stoichiometric subspace is the same as the rank of the reaction network s defined earlier. This was just to illustrate the usefulness of ideas mentioned so far while giving some idea of how a reaction network governs the differential equations and their solution space.

Suppose we want to know what pair of steady-states are possible for our model system. Writing the differential equations for our model (Eqn.[A.6]):

$$\begin{aligned} \dot{cp} &= k1 \cdot m \cdot c - k2 \cdot cp \cdot ppab, & cp + c &= Tc, \\ \dot{m} &= k3 \cdot cp \cdot mp - k4 \cdot m \cdot w, & mp + m &= Tm, \\ \dot{w} &= k6 \cdot wp \cdot pp3 - k5 \cdot m \cdot w, & wp + w &= Tw. \end{aligned} \tag{A.6}$$

Now, let us set the derivatives in Eqn. [A.6] to zero, and let $\mu_\theta \equiv ln({c_\theta}^{**}/{c_\theta}^{*})$, where $\theta = m, mp, c, cp, w, wp, ppab, pp3$, and ${c_\theta}^{**}, {c_\theta}^{*}$ are the two steady-states. We get:

$$\begin{aligned} \mu_m + \mu_c &= \mu_{cp} + \mu_{ppab}, \\ \mu_m + \mu_w &= \mu_{cp} + \mu_{mp}, \\ \mu_m + \mu_w &= \mu_{wp} + \mu_{pp3}. \end{aligned} \tag{A.7}$$

For any two steady-states of the reaction network Eqn.[A.7] must hold. These conditions indicate a connection between steady-state pairs that is independent of rate constants of the network. CRNT treats this as a "signature" of the reaction network. Note that the μs (linear forms) in the signature are related directly to the complexes of the network. For each complex, like $m + c$, we have a corresponding linear form, $\mu_m + \mu_c$. From Eqn.[A.4], we see that our model network has a deficiency of 3 ($n = 10, l = 4, s = 3$). It is a case for the application of Advanced Deficiency Theory that was developed more recently (Ellison, 1998). This theory produces signature(s) relating the μ's of a reaction network. If a network has the capacity to produce multiple steady states, only then will the theory produce a signature for the network. This signature may sometimes contain non-linear equalities. If a signature is produced, the theory has a means to produce an example set of multiple steady-states and corresponding rate constants. Suppose we have (even fragmentary) data about the multiple steady-states of this network. This can be verified against the signature of the network. This provides a means to check if the reaction mechanism proposed in the network is consistent with experimental observations.

Application of advanced deficiency theory, checking existence of multiple steady states, calculation of network signatures and of example rate constants is quite involved. Since these details cannot be presented here in brief, kindly refer Ellison (1998) for the details. Below we show the signature produced using CRNT for our example network. Note that the signature produced agrees with that shown in Eqn.[A.7].

```
                          ============================
                          ADVANCED DEFIENCY REPORT: MCW2
                          ============================

                                 Signature No. 1

                                    m + c = M1
                                  cp + mp = M2
                                cp + ppab = M1
                                    m + w = M2
                                    m + w = M3
                                 wp + pp3 = M3
                                      ppab = 0
                                       pp3 = 0
[m, c, cp, ppab, mp, w, wp, pp3] = [  3.0,  -1.0,   2.0,   0.0,
-1.0,  -2.0,   1.0,   0.0]
```

```
[M1, M2, M3] = [  2.0,   1.0,   1.0]

    Here's an example of a mass action system that gives rise to a pair
of steady states that comply with Signature No. 1:

                  Example No. 1: Multiple Steady States

     The following mass action system gives rise to multiple steady states:

                        m + c --149.87687--> m + cp
                     cp + ppab --18.181266--> c + ppab
                       mp + cp --50.172638--> m + cp
                         m + w --41.927659--> mp + w
                         m + w --41.927659--> m + wp
                      wp + pp3 ------1------> pp3 + w

     The steady states shown below are both consistent with the mass
action system indicated.

    Steady State No. 1            Species            Steady State No. 2

        1.2001 E-2                  m                   0.24106611
        0.36237413                  c                   0.13330999
        3.5852 E-2                  cp                  0.26491671
            1                      ppab                     1
        0.36237413                  mp                  0.13330999
         1.295362                   w                   0.17530819
        0.65184527                  wp                  1.7718991
            1                      pp3                      1

                    Eigenvalues for Steady State No. 1
                                -114.40164
                                -6.3506027
                                 1.7153848
                      Steady State No. 1 is unstable.

                    Eigenvalues for Steady State No. 2
                                -89.043402
                                -34.936171
                                -8.0466516
                Steady State No. 2 is asymptotically stable.
_____________________ Advanced Deficiency Report for CRNT model _____________________
```

Analysis and modification of our model network

We have seen that the simple model presented above is capable of multiple steady states. In this section we use bifurcation analysis of the model to check for bistable nature. Below is the '.ode' file that was used in XPPAUT for bifurcation analysis of our model. Figure [A.1] shows the 1 parameter

bifurcation diagram of above model with respect to the parameter for total-MPF (Tm).

```
# xpp model derived from CRNT model MCW2, a simplified version of
# model MCW_1 without the Enz-Subs complexes.

p k1=149.87687, k2=18.181266, k3=50.172638, k4=41.927659, \
k5=41.927659, k6=1, ppab=1, pp3=1
p Tm=0.3, Tc=1.0, Tw=1.0

mp=Tm-m
c=Tc-cp
wp=Tw-w

cp'= k1*m*c - k2*cp*ppab
m'= k3*cp*mp - k4*m*w
w'= k6*wp*pp3 - k5*m*w

i m=0.01, cp=0.1, w=0.9
```

CRNT model in XPPAUT

Figure [A.1] shows that we do not have bistable nature. A look at the model Eqn.[A.6] shows that $m = 0, cp = 0, w = Tw$ is a fixed point of the system. Making $\dot{m} > 0$ at this point may break the transcritical bifurcation along the $m = 0$ axis (see Fig.[A.1]) giving us the other saddle-node bifurcation we need for bistable nature. With this aim, we modified the equation for $\dot{m}$ in Eqn.[A.6] to:

$$\dot{m} = (k3 \cdot cp + k3p)mp - k4 \cdot m \cdot w. \tag{A.8}$$

In other words, we included a basal phosphatase activity on MPF (even in the absence of Cdc25). With $k3p = 0.1$, we get the desired result in the bifurcation diagram (Fig.[A.2]). For better tuning of parameters, this model with bistable nature was then input into the parameter estimator (see next section for details).

A.2 Jason Zwolak's parameter estimator

Below is an overview of the parameter optimization software (by Jason Zwolak) that was used on the simple 3 variable model given by CRNT (see Eqn.[A.6,A.8]). For more details refer Zwolak et al. (2004b,a).

Overview

The primary goal of model building is to minimize the differences between experimental observations and model simulations. However, errors in measurements and inadequacies of the model usually

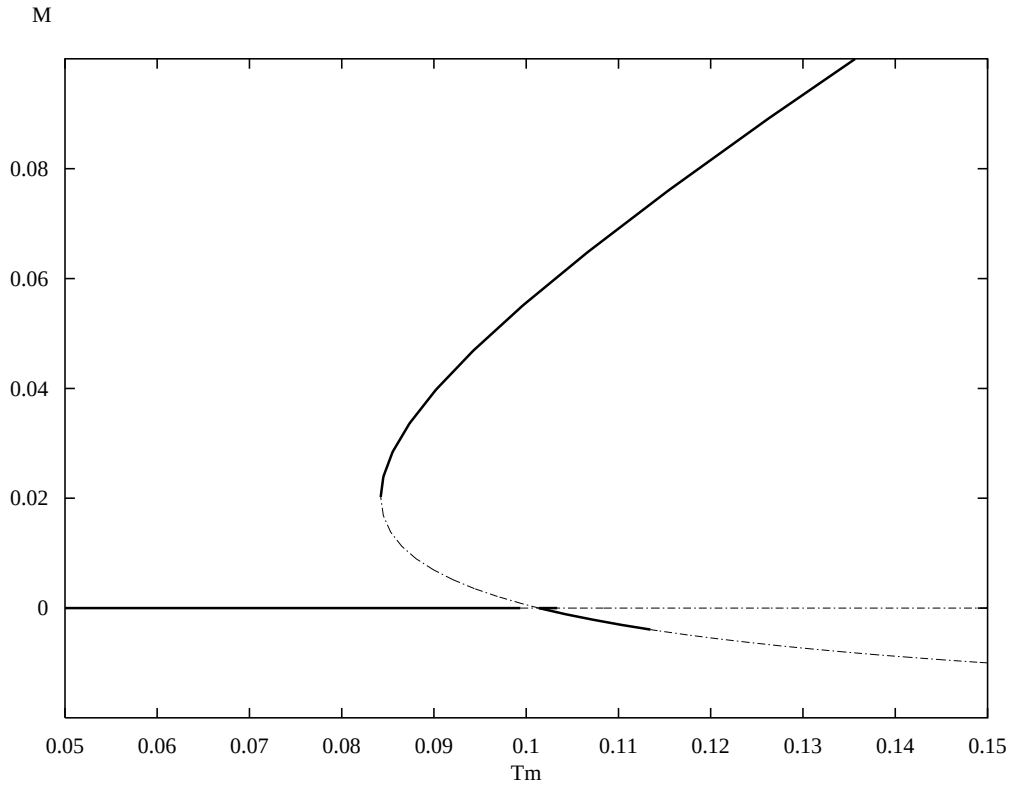

Figure A.1: One parameter bifurcation diagram of the CRNT model in Eqn.[A.6]. Thick lines indicate stable steady-state. Note the *saddle node*, *exchange* (transcritical), and *hopf* bifurcations near $Tm = 0.085, 0.1, 0.115$ respectively.

lead to imperfect match between these two. To minimize this difference using computer programs one usually makes an index for the goodness-of-fit, and then uses it in algorithms that minimize it. (A smaller index meaning better fit.) Let

$$\mathbf{y} = \mathbf{f}(\mathbf{x}; \beta) \tag{A.9}$$

represent our model's output (with $[\mathbf{x}; \beta]$ as inputs), where $\mathbf{y},\ \mathbf{x},\ \beta$ are vectors. Let $\bar{x}_i,\ \bar{y}_i$ represent the experimental observations. Note that if the measurements were made for checking some qualitative behaviour, usually both $\bar{x}$ and $\bar{y}$ will have measurement errors. Consider, for instance, the experiments where a fixed amount of non-degradable cyclin is added to extracts and the time-lag for entry into mitosis is measured (refer Fig.[4.4b]). Here, the time-lag is infinite for certain (low) amounts of cyclin, and this would clearly lead to huge errors if we did not consider errors in measurement of cyclin amounts by using the orthogonal distance between data and simulation results. Thus, for every experimental data point $\{\bar{x}_i,\ \bar{y}_i\}$, we aim to minimize $(y - \bar{y}_i)^2 + (x - \bar{x}_i)^2$, the distance between this point and the model result. The following function, commonly called a "cost" or "penalty" function, gives a positive scalar index of the goodness-of-fit of all data points with the model:

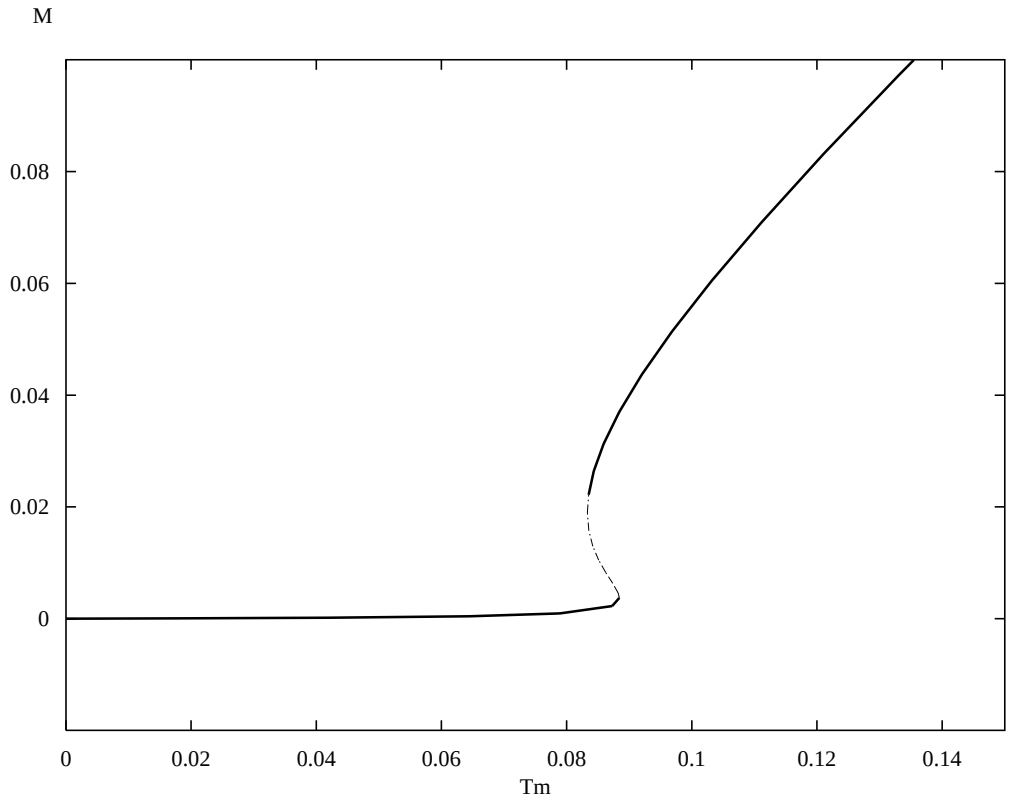

Figure A.2: One parameter bifurcation diagram of modified CRNT model. Thick lines indicate stable steady-state. Note the appearance of a *saddle node* bifurcation near the location of the *exchange* bifurcation in Fig.[A.1].

$$E_{min} = \min_{\delta,\beta} \left(\sum_{i=1}^{n} w_{\epsilon_i} \epsilon_i^2 + w_{\delta_i} \delta_i^2 \right), \tag{A.10}$$

with $\epsilon_i = f_i(x_i + \delta; \beta) - y_i, i = 1, \ldots, n$. δ_i and ϵ_i are discrepancies in x and y, while w_{δ_i} and w_{ϵ_i} are the respective weights for these errors. The weights allow us to express our confidence in particular data and also to convert them into common "currency". Since the cost function measures the perpendicular (hence minimum) distance of each data point from model solution, this method is termed Orthogonal Distance Regression (ODR).

Now, given a starting point and a region in parameter space, we need to take steps so that the cost function is minimized. Local methods aim to find the best point in the neighborhood of the starting point and stop when everything close by only worsens the fit. Global methods have the ability to look beyond local minima of the cost function. Each step of either algorithm depends on the previous step(s). This dependence on previous steps may either be deterministic or stochastic. The parameter optimizer used here uses deterministic global and local methods.

Note that for optimizing our ODE based model, we need 2 components:

Parameter name (old) [1]	Initial value (CRNT)	Optimized value	Final value (in new model)	Corresponding parameter name (new) [2]
$k1$	149.877	6.76	6.485	$kc285$
$k2$	18.181	0.081	0.0859	$rkc285 \cdot kc285$
$k3$	50.173	0.1618	0.45	km
$k3p$	0.1	0.000976	0.0032	$rkmc \cdot km$
$k4$	41.928	23.1	8.55	$rkm \cdot km$
$k5$	41.928	713.2	1.35	$rkw\_mpf \cdot kw\_mpf$
$k6$	1	0.114	0.27	kw_mpf

Table A.1: Parameter optimization: from initial to final values. For old parameter names in the first column, refer CRNT model in XPPAUT shown towards the end of section [A.1]. For new parameter names in the last column, refer Eqn.[3.1 – 3.13] on pg. 23.

- A means to find $\mathbf{y}_i$ at a given point $[\mathbf{x}_i; \beta]$, i.e., an ODE integrator; and
- An algorithm to take appropriate steps in the parameter space, i.e., the global and/or local optimizer.

This optimizer uses the public domain softwares LSODAR, ODRPACK, and VTDIRECT for integrating the ODEs, local optimization, and global optimization respectively. LSODAR has the ability to integrate stiff ODEs and finding roots. ODRPACK uses a trust region Levenberg-Marquardt method with scaling to minimize E (see Eqn.[A.10]). For some details of the algorithm used for local optimization please refer Zwolak et al. (2004b). Zwolak et al. (2004a) gives an outline of how the VTDIRECT algorithm for global optimization works. For our model, we used the experimental data shown in Figures [4.2, 4.3, 4.4]. This is (almost) same as the data appearing in Zwolak et al. (2004b, Tab. 3); the same weights as in this table were used in our computations.

Output of parameter optimization

The model that was input to the parameter estimation was same as shown previously in the `XPPAUT` code with the modification of $\dot{m}$ equation to Eqn.[A.8]. Table [A.1] shows the initial parameter values, optimized values, and the final values for corresponding parameters in the complete model.

Bibliography

D. Bulavin, Z. Demidenko, C. Phillips, S. Moody, and A. J. Fornace. Phosphorylation of *Xenopus* Cdc25C at Ser285 interferes with ability to activate a DNA damage replication checkpoint in pre-midblastula embryos. *Cell Cycle*, 2(3):263–266, May 2003a.

D. Bulavin, Y. Higashimoto, Z. Demidenko, S. Meek, P. Graves, C. Phillips, H. Zhao, S. Moody, E. Appella, H. Piwnica-Worms, and A. J. Fornace. Dual phosphorylation controls Cdc25 phosphatases and mitotic entry. *Nature Cell Biology*, 5(6):545–551, June 2003b.

M. Dasso and J. Newport. Completion of DNA replication is monitored by a feedback system that controls the initiation of mitosis in vitro: studies in Xenopus. *Cell*, 61(5):811–23, July 1990.

R. P. Elinson. Xenopus as and Experimental Organism. *Nature Encyclopedia of Life Sciences*, Jan. 2003. London: Nature Publishing Group. http://www.els.net/ [doi:10.1038/npg.els.0002030].

P. R. Ellison. The Advanced Deficiency Algorithm and its Applications to Mechanism Discrimination. 1998. Ph.D. Thesis, Dept. of Chemical Engg., Univ. of Rochester.

B. Ermentrout. *Simulating, Analyzing, and Animating Dynamical Systems A guide to XPPAUT for Researchers and Students*. SIAM, 2002. Refer http://www.math.pitt.edu/ bard/xpp/xpp.html for more information and free download of XPPAUT software.

M. Feinberg. Chemical Reaction Network Structure and the Stability of Complex Isothermal Reactors – I. The Deficiency Zero and Deficiency One Theorems. *Chemical Engineering Science*, 42(10):2229–68, 1987. Review.

M. Feinberg. Chemical reaction network structure and the stability of complex isothermal reactorsII. Multiple steady states for networks of deficiency one. *Chemical Engineering Science*, 43(1): 1–25, 1988. Review.

M. Feinberg. Multiple Steady States for Chemical Reaction Networks of Deficiency One. *Archive for Rational Mechanics and Analysis*, 132:371–406, 1995a.

M. Feinberg. The Existence of Uniqueness of Steady States for a Class of Chemical Reaction Networks. *Archive for Rational Mechanics and Analysis*, 132:311–370, 1995b.

M. Feinberg and P. R. Ellison. The Chemical Reaction Network Toolbox. *http://www.che.eng.ohio-state.edu/˜feinberg/crnt/*, 1999. (v1.1a, download CRNT program and manual).

Z. Guo, A. Kumagai, S. Wang, and W. Dunphy. Requirement for Atr in phosphorylation of Chk1 and cell cycle regulation in response to DNA replication blocks and UV-damaged DNA in Xenopus egg extracts. *Genes Dev.*, 14(21):2745–56, Nov. 2000.

D. Hanahan and R. A. Weinberg. The Hallmarks of Cancer. *Science*, 100:57–70, Jan. 2000. Review.

L. Hartwell and T. Weinert. Checkpoints: controls that ensure the order of cell cycle events. *Science*, 246(4930):629–634, Nov. 1989. Review.

T. Hunter. Signaling – 2000 and beyond. *Cell*, 10:113–127, 2000. Review.

T. Izumi and J. L. Maller. Elimination of cdc2 phosphorylation sites in the cdc25 phosphatase blocks initiation of M-phase. *Molecular Biology of the Cell*, 4(12):1337–50, Dec. 1993. http://www.molbiolcell.org.

P. Kaldis. The cdk-activating kinase (CAK): from yeast to mammals. *Cell. Mol. Life Sci.*, 55(2): 284–96, Feb. 1999. Review.

A. Kumagai and W. Dunphy. The cdc25 Protein Controls Tyrosine Dephosphorylation of the cdc2 Protein in Cell-Free System. *Cell*, 64:903–914, Mar. 1991.

A. Kumagai and W. Dunphy. Regulation of the cdc25 protein during the Cell Cycle in Xenopus extracts. *Cell*, 70(1):139–151, July 1992.

A. Kumagai and W. Dunphy. Control of the Cdc2/Cyclin B complex in Xenopus Egg Extracts Arrested at a G2/M Checkpoint with DNA Synthesis Inhibitors. *Molecular Biology of the Cell*, 6(2):199–213, Feb. 1995. http://www.molbiolcell.org.

A. Kumagai and W. Dunphy. Binding of 14-3-3 proteins and nuclear export control the intracellular localization of the mitotic inducer Cdc25. *Genes & Dev.*, 13(9):1067–72, May 1999.

A. Kumagai, Z. Guo, K. Emami, S. Wang, and W. Dunphy. The Xenopus Chk1 protein kinase mediates a caffeine-sensitive pathway of checkpoint control in cell-free extracts. *The Journal of Cell Biology*, 142(6):1559–1569, Sept. 1998a.

A. Kumagai, P. Yakowec, and W. Dunphy. 14-3-3 proteins act as negative regulators of the mitotic inducer Cdc25 in Xenopus egg extracts. *Molecular Biology of the Cell*, 9(2):345–354, Feb. 1998b. http://www.molbiolcell.org.

J. Lee, A. Kumagai, and W. G. Dunphy. Positive Regulation of Wee1 by Chk1 and 14-3-3 Proteins. *Molecular Biology of the Cell*, 12:551–563, Mar. 2001. http://www.molbiolcell.org.

D. J. Lew and S. Kornbluth. Regulatory roles of cyclin dependent kinase phosphorylation in cell cycle control. *Current Opinion in Cell Biology*, 8:795–804, 1996. Review.

H. Lodish, A. Berk, P. Matsudaira, C. A. Kaiser, M. Krieger, S. L. Zipursky, and J. Darnell. *Molecular Cell Biology*. W. H. Freeman & Co., New York, 5 edition, 2003.

S. Margolis, S. Walsh, D. Weiser, M. Yoshida, S. Shenolikar, and S. Kornbluth. PP1 control of M phase entry exerted through 14-3-3 regulated Cdc25 dephosphorylation. *EMBO J.*, 22(21): 5734–45, Nov. 2003.

G. Marlovits, C. Tyson, B. Novak, and J. Tyson. Modeling M-phase control in Xenopus oocyte extracts: the surveillance mechanism for unreplicated DNA. *Biophysical Chemistry*, 72(1):169–184, May 1998.

J. Moore. Private Communication. Aug. 1997.

D. O. Morgan. CYCLIN-DEPENDENT KINASES: Engines, Clocks, and Microprocessors. *Annual Review in Cell and Developmental Biology*, 13:261–91, 1997. Review.

P. Mueller, T. Coleman, and W. Dunphy. Cell cycle regulation of a Xenopus Wee1-like kinase. *Molecular Biology of the Cell*, 6(1):119–134, Jan. 1995a. http://www.molbiolcell.org.

P. Mueller, T. Coleman, A. Kumagai, and W. Dunphy. Myt1: a membrane-associated inhibitory kinase that phosphorylates Cdc2 on both threonine-14 and tyrosine-15. *Science*, 270(5233):86–90, Oct. 1995b.

E. A. Nigg. Mitotic Kinases as Regulators of Cell Division and its Checkpoints. *Nature Reviews Molecular Cell Biology*, 2:21–32, Jan. 2001.

B. Novak, J. Sible, and J. Tyson. Checkpoints in the Cell Cycle. *Nature Encyclopedia of Life Sciences*, Sept. 2002. London: Nature Publishing Group. http://www.els.net/ [doi:10.1038/npg.els.0001355].

B. Novak and J. J. Tyson. Numerical analysis of a comprehensive model of M-phase control in Xenopus oocyte extracts and intact embryos. *Journal of Cell Science*, 106(4):1153–1168, Dec. 1993.

K. Nyberg, R. Michelson, C. Putnam, and T. Weinert. Toward maintaining the genome: DNA damage and replication checkpoints. *Annu. Rev. Genet.*, 36:617–56, 2002. Review.

J. Pomerening, E. Sontag, and J. J. Ferrell. Building a cell cycle oscillator: hysteresis and bistability in the activation of Cdc2. *Nature Cell Biology*, 5(4):346–51, Apr. 2003.

M. H. Regenmortel. Reductionism and complexity in molecular biology. *EMBO Reports*, 5(11): 1016–20, 2004. Review.

A. Sancar, L. Lindsey-Boltz, K. Unsal-Kaccmaz, and L. S. Molecular mechanisms of mammalian DNA repair and the DNA damage checkpoints. *Annu. Rev. Biochem.*, 73:39–85, 2004. Review.

W. Sha, J. Moore, K. Chen, A. Lassaletta, C. Yi, J. Tyson, and J. Sible. Hysteresis drives cell-cycle transitions in Xenopus laevis egg extracts. *Proc. Natl. Acad. Sci. U S A.*, 100(3):975–980, Feb. 2003.

M. Solomon, M. Glotzer, T. Lee, M. Philippe, and M. Kirschner. Cyclin activation of p34cdc2. *Cell*, 63(5):1013–24, Nov. 1990.

Z. Tang, T. Coleman, and W. Dunphy. Two distinct mechanisms for negative regulation of the Wee1 protein kinase. *EMBO J.*, 12(9):3427–36, Sept. 1993.

K. Uto, D. Inoue, K. Shimuta, N. Nakajo, and N. Sagata. Chk1, but not Chk2, inhibits Cdc25 phosphatases by a novel common mechanism. *EMBO J.*, 23(16):3386–96, Aug. 2004.

N. C. Walworth. DNA damage: Chk1 and Cdc25, more than meets the eye. *Current Opinion in Genetics & Development*, 11:78–82, 2001. Review.

B.-B. S. Zhou and S. J. Elledge. The DNA damage response: putting checkpoints in perspective. *Nature*, 408(6811):433–9, Nov. 2000. Review.

J. W. Zwolak, J. J. Tyson, and L. T. Watson. Globally Optimized Parameters For a Xenopus Egg Extract Model. 2004a. in preparation (draft).

J. W. Zwolak, J. J. Tyson, and L. T. Watson. Parameter Estimation for a Mathematical Model of the Cell Cycle in Frog Eggs. *Journal of Computational Biology*, 2004b. to appear.

Vita

Amit Dravid was born on 19 January 1978 in India. He obtained his Bachelor of Engineering in Electrical Engineering from the Sardar Pater University, Vallabh Vidyanagar, India in Dec 2000. He worked as a software engineer for 1.5 years before starting on his graduate education. In the fall-term of 2002, he joined the lab of Dr. John J. Tyson at Virginia Tech and has been there ever since.